MODELLING OF EARTHQUAKE INDUCED OVERTURNING OF BUILDING CONTENTS

HAIDER A. AL ABADI[1], NELSON T.K. LAM[1], EMAD F. GAD[2] AND ADRIAN M. CHANDLER[3]

AUTHORS:

1. Department of Civil & Environmental Engineering, University of Melbourne, Victoria, Australia.
2. Swinburne University of Technology and University of Melbourne, Victoria, Australia.
3. Department of Civil Engineering, University of Hong Kong.

ABSTRACT

Damage to critical contents in buildings following an earthquake (or explosion) often results in significant economic losses if the building cannot perform its normal functions over an extended period of time. Building codes have begun to address potential damage to building contents, but this has been handicapped by the lack of knowledge on their potential behaviour in an extreme event. The conventional force-based approach of estimating the peak floor acceleration and the associated inertia forces on an object is unrealistic, as the components are often unrestrained. Clearly, the normal assumption that "*building content is part of the building's primary structure (i.e. fixed components)*" is inappropriate.

This paper introduces a rational procedure to model the rocking response behaviour of free-standing objects when subjected to earthquake excitations. This new method utilizes the displacement-based approach and presents results in the form of Rocking Displacement Spectra (RDS). The RDS is different to the Displacement Response Spectra in that, the displacement demand is calculated from non-linear time-history analyses and results are expressed as a function of the object dimensions (i.e. thickness and height) as opposed to the object natural period. Given a certain excitation on a building floor, the RDS provides a direct indication of the maximum displacement experienced by a range of components, and quantifies their risk of overturning. The RDS format represents a significant step forward in modelling overturning of building contents.

1. INTRODUCTION

The development of analytical techniques in current buildings standards (including the Australian Earthquake Standard, AS 1170.4, 1993), for free standing objects has mirrored that for the primary structure of buildings. Most of these techniques use equivalent lateral force methods (i.e. force based approach), where the components are designed for a lateral seismic force that is expressed as the product of the component mass and the Peak Floor Acceleration (PFA) developed in the component according to basic principles of mechanics. The PFA at any level in the building is obtained by linear interpolation between acceleration estimated at the roof and ground level (e.g. FEMA 356, 2000; IBC, 2000 and AS 1170.4,1993). The value of the design PFA at the roof of the building may be estimated by taking the ratio of the estimated inertia force acting at the roof level and the mass of the roof.

The objective of this conventional force based design approach is to produce an anchorage or bracing scheme for the components that can withstand the acceleration generated by the earthquake, without allowing the component to shift or topple. Accordingly the analytical techniques for assigning the response of components, which are demonstrated by recent building standards, assume that components would be fully restrained.

In regions of low to moderate seismicity including Australia, the provision of holding-down fasteners to secure building contents is not common. Computer cabinets and electrical components are typically free-standing and without any holding-down fasteners (Al Abadi et al, 2003). Enforcing full restraints on every item of equipment in every facility is desirable but has never been implemented in Australia, and yet failure or damage to building contents in an earthquake (or explosion) could disturb the continuos functioning and subject its occupants to significant risks even in a moderate earthquake. Hence, this paper focuses on the response of free-standing objects, which are free-standing and without effective hold-down connections.

The concept of using displacement spectra (i.e. displacement based DB approach) to model the behaviour of the unrestrained component is introduced in this paper by a new rational approach, which presents results in the form of Rocking Displacement Spectra (RDS).

The RDS is a plot of the maximum object displacement, versus the parameter R (distance between the object centre of mass to the pivotal edge) for different object thicknesses.

Given the basic parameters of an object, RDS can be used directly to predict whether components will overturn or rock. And for the rocking scenario, RDS can predict the component maximum displacement.

In this paper, a brief review for the Elastic Displacement Spectra approach is presented in Section 2. Section 3 presents the background and development of the Rocking Displacement Spectra (RDS) approach.

2. ELASTIC DISPLACEMENT SPECTRA (EDS) APPROACH

It has been found from a recent investigation (Al Abadi et al, 2004) into the response of slender free-standing rectangular objects that the maximum displacement developed in a rocking motion can be reasonably approximated by the motion predicted for a Single-Degree-Of-Freedom (SDOF) lumped mass system, as shown schematically in Fig.1a.

The force-displacement relationship representing the response to a push-over load is shown in Fig. 1b (refer line drawn in bold). Using substitute-structure modelling, the force-displacement behaviour could be linearized with an effective stiffness. Accordingly the effective period (or T_{eff}) of rocking could be estimated by the formula shown in Fig. 1. It should be noted that the highest point on the displacement spectrum does not necessarily appear as a prominent peak when plotted in the conventional acceleration response spectrum format. Thus, the described approach of tracking the maximum displacement demand from a displacement spectrum would not have been possible using the acceleration response.

$$\text{Effective period} = T_{eff} = 2\pi\sqrt{\frac{M_e}{k_e}} = 2\pi\sqrt{\frac{\frac{3}{4}M}{\frac{9}{8}\frac{Mg}{H}}} = 2\pi\sqrt{\frac{2}{3}\frac{H}{g}}$$

M = component mass
M_e = effective mass
Δ_e = effective displacement
H = components height
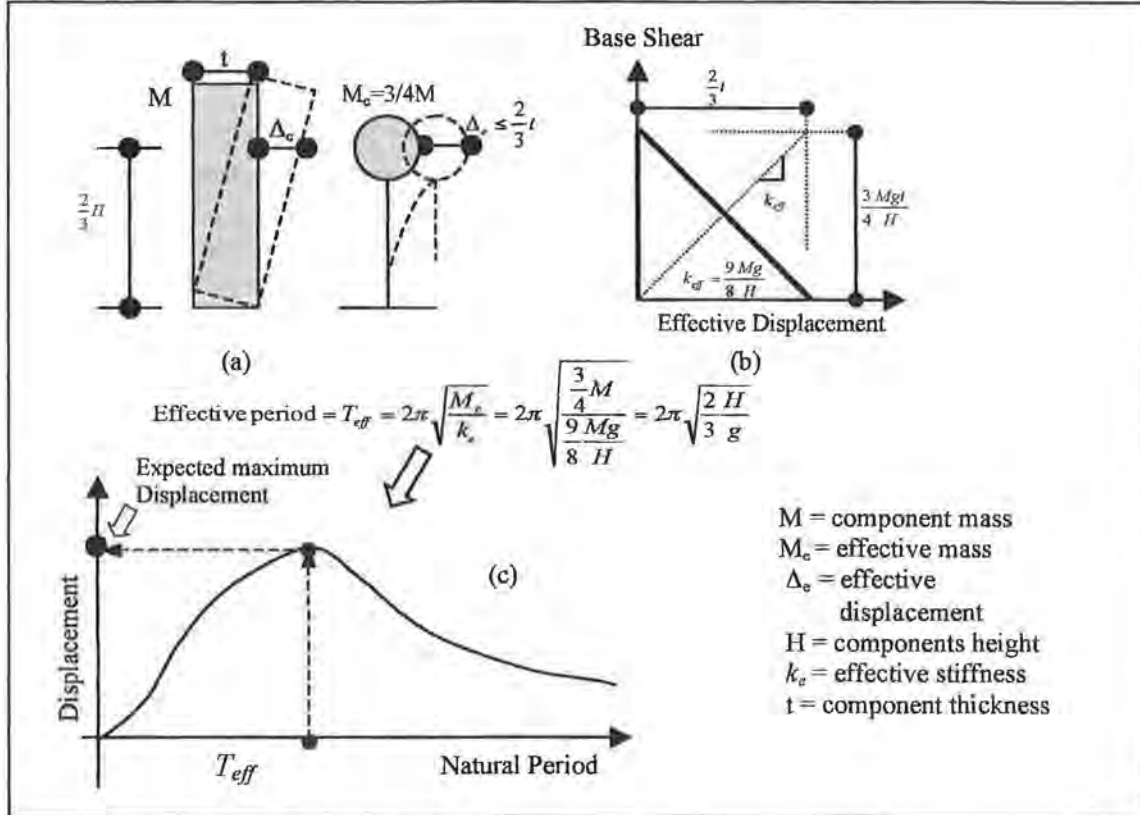k_e = effective stiffness
t = component thickness

Fig. 1: Elastic displacement spectra for rocking response.

This simplified method of using an elastic displacement spectrum to predict the displacement of a rocking object by substitute-structure modelling, is only meant to provide an approximation to the actual response. The modelling is particularly susceptible to significant errors when the response is highly non-linear. This is discussed further in the following section.

3. ROCKING DISPLACEMENT SPECTRA (RDS) APPROACH

Rocking response for rigid bodies had been subjected to extensive study, as reviewed by Makris and Roussos (1998). This paper presents only the development of the rocking spectra concept. Research on the development of rocking spectra has recently been conducted by Makris and Konstantinidis (2001) in studying the response of ground mounted electrical transformers. In their study, the proposed rocking spectra were plots

of the maximum rotation, θ, versus the frequency parameter, p (or its inverse "Time period, $T=2\pi/p$").

The Rocking Displacement Spectra (RDS) approach is presented herein as a function of the object dimensions (i.e. thickness, height) as opposed to the object natural period.

To show the development of RDS, a rigid block as shown in Fig. 2 is considered. Two main assumptions are applied to the model, which are: (i) the magnitude of horizontal acceleration is sufficiently large enough to cause initial rocking; (ii) the coefficient of friction is large enough so that there is no sliding. Complex motions such as "walking" have been ignored at this stage of the investigation. Under a positive horizontal acceleration that is sufficiently large, a rigid block will initially rotate with a negative rotation, $\theta < 0$ and, if it does not overturn, it will eventually assume a positive rotation; and so on. Uniform distribution of mass is also assumed so that the centre of mass of the object is also at its geometric centre. Investigation is continued to address objects with non-uniform distribution of mass.

The equations that govern the rocking motion under horizontal ground/floor acceleration $\ddot{u}_g(t)$ are

$$I_o\ddot{\theta}(t) + MgR\sin(-\theta_{cr} - \theta(t)) = -M\ddot{u}_g(t)R\cos(-\theta_{cr} - \theta(t)), \quad \theta(t) < 0 \tag{1}$$

and

$$I_o\ddot{\theta}(t) + MgR\sin(\theta_{cr} - \theta(t)) = -M\ddot{u}_g(t)R\cos(\theta_{cr} - \theta(t)), \quad \theta(t) > 0 \tag{2}$$

where I_o is the mass moment of inertia about the centre of rotation, $\ddot{\theta}$ is the angular acceleration, M is the mass of the block, g is gravitational acceleration, R ($R = \sqrt{(h/2)^2 + (t/2)^2}$), is the distance from the centre of mass to the pivot edge (see Fig. 2), θ_{cr} is the critical overturning angle, and θ is the rotation angle.

Eqs. 1 and 2 have been adopted in similar research (Yim *et* al 1980, Makris and Roussos 2000, among others) and are valid for arbitrary values of the critical angle θ_{cr} ($\theta_{cr} = \tan^{-1}(t/h)$). The frequency parameter, p, for the rocking component is defined as $p = \sqrt{MgR/I_o}$, $I_o = (4/3)MR^2$ for rectangular blocks. Hence the frequency parameter can be simplified to $\sqrt{3g/4R}$ for rectangular objects. It should be noted that the frequency parameter formula is different than the one predicted in the EDS modelling (refer to Fig. 1), which is a function only of the height of the component (i.e. $p = \sqrt{3g/2H}$), in

Fig. 2. Dimensions and parameters used to describe the rocking of a block.

which an assumption of $R=h/2$ was adopted. This assumption limits the EDS model to very slender objects (e.g. walls). In the new RDS model the frequency parameter (p) is applicable to any level of slenderness.
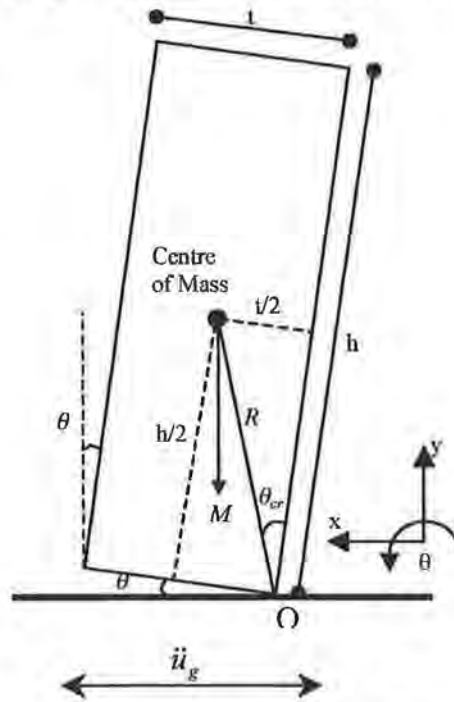
Eqs. 1 and 2 can be expressed in the compact form:

$$\ddot{\theta}(t) = -p^2 \{\sin[\theta_{cr} \operatorname{sgn}[\theta(t)] - \theta(t)] + \frac{\ddot{u}_g}{g} \cos[\theta_{cr} \operatorname{sgn}[\theta(t)] - \theta(t)]\} \tag{3}$$

or

$$\ddot{\theta}(t) = -\frac{3}{4R} \{g \sin[\theta_{cr} \operatorname{sgn}[\theta(t)] - \theta(t)] + \ddot{u}_g \cos[\theta_{cr} \operatorname{sgn}[\theta(t)] - \theta(t)]\} \tag{4}$$

The solution of the nonlinear problem of Eq. 4, need to be adjusted by accounting for the energy loss at every ground impact during rocking. The conservation of angular momentum principle (Ferdinand et al, 2004) could be applied at the instant of impact for predicting the dissipation in energy in terms of coefficient of restitution (R_D), as shown by Eq. 5.

$$R_D = \frac{\text{Angular velocity after impact}}{\text{Angular velocity befor impact}} = \frac{\dot{\theta}_2}{\dot{\theta}_1} = \frac{\dfrac{2R^2 - t^2}{2} + \dfrac{R^2}{3}}{R^2 + \dfrac{R^2}{3}} \tag{5}$$

The numerical integration of Eq. 4 along with the condition expressed by Eq. 5 yields the rotation time-history of a block for a given value for R, block thickness t, and ground excitation.

The solution algorithm for these equations can be implemented using a program language such as Fortran or C. In this research, Matlab has been used.

To illustrate the form and use of the RDS, a single pulse is applied as the ground or floor excitation. The displacement pulse and corresponding acceleration pulse are shown in Figs. 3a and 3b, respectively. Fig. 3c shows the resulting RDS for a rectangular component with different thicknesses (t) varying from 400mm to 1000mm (the vertical axis of Fig. 3c and 4, presents the effective displacement that is defined at two-third the height of the object).

It can be seen from Fig. 3c, RDS provides direct prediction of rocking response for a given object, using only two geometric parameters (R and t). The RDS directly presents the critical range of thicknesses for overturning, as illustrated for objects with thickness of 400mm.

Fig. 4 shows RDS for rectangular objects excited by an earthquake scenario. Similarly, Fig. 4 shows directly whether component would overturn or would rock. For the rocking situation, the maximum displacement at the effective height can be obtained.

In Figs. 3c and 4 the Elastic Displacement Spectra (EDS) are shown, to highlight the difference in prediction using these two methods. These two figures shows that the EDS can be highly non-conservative in predicting displacement, and hence the risk of overturning. Fig. 3c indicates that RDS predicts maximum displacement that is about twice that predicted by EDS. This ratio is found associated with only single pulse excitation and will be different with earthquake excitation, as illustrated by the comparison between RDS and EDS shown in Fig. 4. In this paper, only one accelerograms has been used to illustrate the effects of earthquake excitations characteristics by multiple cycles of pulse. Investigation is continuing with the use of accelerograms, which account for the filtering effects of the building.

Significantly, the RDS presentation can directly predict the minimum thickness of a component that will not overturn under a given excitation. For example, components with thickness greater than 600mm would not overturn when subjected to a single pulse

excitation (refer to Fig. 3c), while for the earthquake excitation, components with thickness more than 800mm are safe from overturning (refer to Fig. 4).
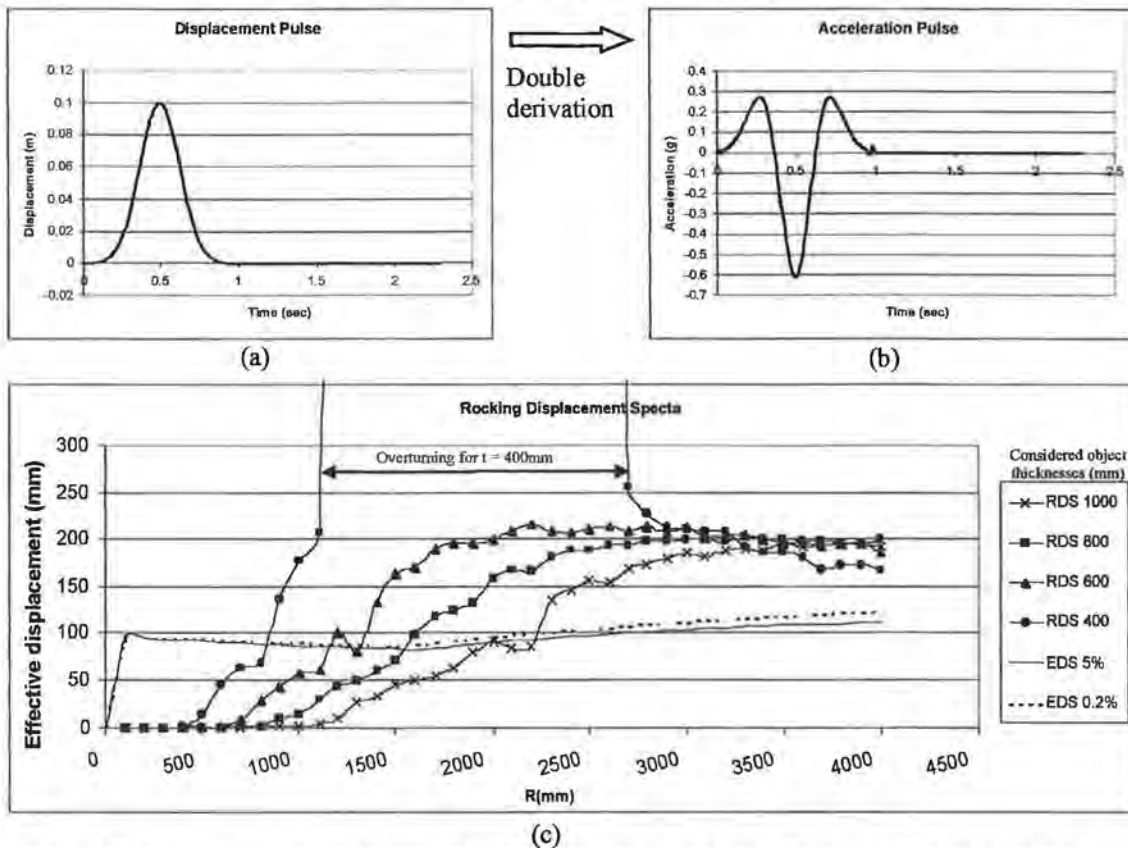

(a)

(b)

(c)

Fig. 3. Rocking Displacement Spectra (RDS) for a rectangular block with thicknesses of t = 400 to 1000mm, generated by single displacement pulse (shown below).
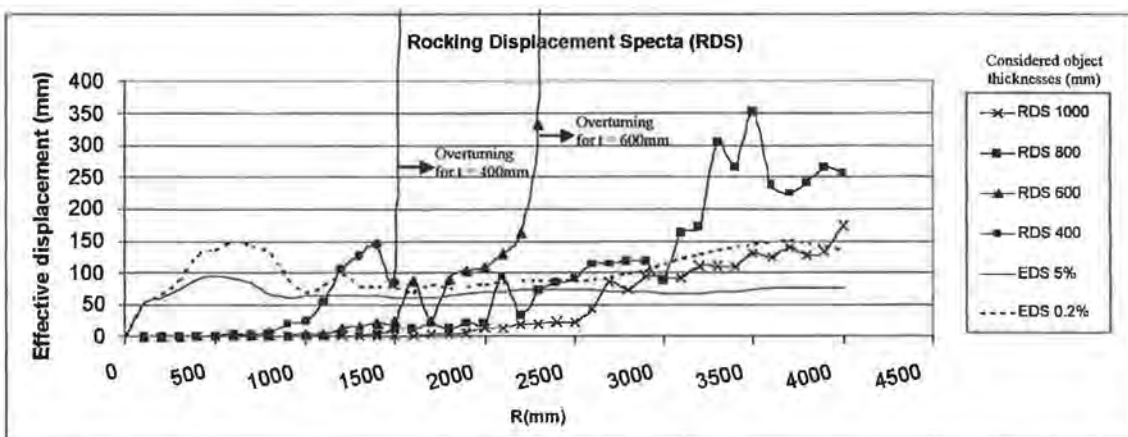

Fig. 4. Rocking Displacement Spectra (RDS) for a rectangular block with thicknesses of t = 400 to 1000mm, subjected to the 1940 El Centro (NS) California earthquake excitation.

4. CONCLUSIONS

The modelling of the behaviour of unrestrained components subjected to earthquake (or explosion) excitation in buildings by a rational procedure has been considered in this

paper. A brief overview of the Elastic Displacement Spectra (EDS) approach for predicting the rocking response was presented and its limitations highlighted.

The new approach is performed by modelling the rocking problem in its real nonlinear form and also by applying the damping to the rocking motion at each impact during the rocking. With these procedures the exact Rocking Displacement Spectra (RDS) are predicted as a function of the component dimensions (i.e. thickness and height) as opposed to the object natural period in the EDS plot. Given a certain excitation on a building floor, RDS provides a direct indication of whether a component with specific dimensions will overturn or rock. For the rocking response case, RDS can show the maximum displacement expected during that excitation.

The use of RDS would enable direct and accurate assessment of free-standing equipment, particularly for the risk for overturning.

5. ACKNOWLEDGMENTS

6. REFERENCES

Al Abadi, H., Gad, E., Lam, N.T.K., & Chandler, A.M. 2003. Risks from the Response of the Non-structural Components to Seismic Loads in Buildings. *Proceeding of the Annual conference of the Australian Earthquake Engineering Society*: 27-28.

Al Abadi, H., Gad, E., Lam, N.T.K., & Chandler, A.M. 2004. Earthquake Floor Spectra for Unrestrained Building Components. *International Journal of Structural Stability and Dynamics* Vol. 4, No. 3.

AS1170.4 (1993) *Standards Association of Australia:* Minimum design loads on structures: Part4: Earthquake Loads – AS1170.4 and Commentary.

FEMA 356. (2000). *Prestandard and Commentary for Seismic Rehabilitation of Buildings.* Prepared by the American Society of Civil Engineers for the Federal Emergency Management Agency. FEMA.

Ferdinand B., Johnston E., & Clausen W. 2004. *Vector Mechanics for Engineers Dynamics.* New York: McGraw-Hill.

IBC (2000) International Code Council. *International building Code*, 2000. U.S.A.

Makris, N. and Roussos, Y. (1998). Rocking Response and Overturning of Equipment Under Horizontal Pulse-Type Motions. *Pacific Earthquake engineering Research center.* PEER, OCT (Report No. 5).

Makris, N. and Roussos, Y. (2000). Rocking Response of Rigid Blocks under Near-Source Ground Motions. *Géotechnique* 50, No. 3, 243-262.

Makris, N. and Konstantinidis, D. (2001). The Rocking Spectrum and Shortcomings of Design Guidelines. *Pacific Earthquake engineering Research center.* PEER, AUG. (Report No. 7).

Yim, S. C. S, Chopra, A. K., and Penzien, J. (1980). Rocking Response of Rigid Blocks to Earthquakes. *Earthquake Engineering and Structural Dynamics* 122(7):69093.ASCE.

SOME EMPIRICAL RELATIONS FOR ATTENUATION OF GROUND-MOTION SPECTRAL AMPLITUDES IN SOUTHWESTERN WESTERN AUSTRALIA

TREVOR ALLEN[1], TREVOR DHU[1], PHIL CUMMINS[1], JOHN SCHNEIDER[1] AND GARY GIBSON[2]

GEOSCIENCE AUSTRALIA[1], ENVIRONMENTAL SYSTEMS AND SERVICES[2]

AUTHORS:

Trevor Allen is a seismologist with the Risk Research Group, GA. He is currently working to develop spectral ground-motion attenuation models for the Australian crust.

Trevor Dhu is a geophysicist with the Risk Research Group, GA. His research is focused on national scale earthquake risk maps as well as developing site response and strong-motion models for Australia.

Phil Cummins is Leader of the Earthquake Hazard and Neotectonics Project at GA. He oversees GA's earthquake monitoring activities and earthquake hazard research.

John Schneider is the Leader of the Risk Research Group, Geoscience Australia. His interests are in the development of natural hazard risk assessment methods for applications to urban centres, with particular emphasis on earthquake hazards.

Gary Gibson established the Seismology Research Centre in 1976 and is an Honorary Research Associate at Monash University. His interests lie in observational seismology and its practical applications.

INTRODUCTION:

Australian earthquake hazard and risk assessments currently suffer from considerable uncertainty since they are forced to rely on ground-motion attenuation models derived in other regions [e.g. eastern North America (ENA)] (Dhu and Jones, 2002; Robinson *et al.*, 2004). These uncertainties can lead to undesirable outcomes, including unrealistically high loading standards in the design and construction of critical infrastructure such as large dams.

Attenuation relations appropriate for the Australian crust have, in the past, been difficult to quantify owing to a lack of ground-motion data from moderate-to-large local earthquakes. Geoscience Australia (GA), in association with Environmental Systems and Services (ES&S) and the Australian National Committee on Large Dams (ANCOLD) are presently collaborating to assemble an Australian ground-motion database suitable for attenuation studies. This paper examines data acquired during the 2001-02 Burakin, Western Australia (WA), earthquake sequence (Leonard, 2003). The dataset represents the largest resource of high sample-rate digital data in WA that is useful for detailed spectral studies of this kind. We estimate source and path parameters, and subsequently perform regressions to define a Fourier spectral attenuation model for the Archean shield region of southwestern WA. For intraplate regions with low levels of seismicity, empirical studies such as this provide key input parameters for stochastic ground-motion generation of larger earthquakes (e.g. Atkinson and Boore, 1995; Toro *et al.*, 1997).

These data present a unique opportunity to study small-to-moderate magnitude earthquakes recorded at very small hypocentral distances. Moreover, the work described will provide a useful framework for developing regional ground-motion relations for Western Australia and the continent as a whole.

TEMPORARY NETWORK AND DATA:

At the onset of activity at Burakin in 2001-02, GA made a concerted effort to deploy a temporary seismic network in the region. The primary objective of this network was to collect high-quality strong-motion data for use in attenuation studies. Of the many thousands of located events, we analyse a subset of 67 earthquakes of **M** 2.3 and greater recorded from 30 September 2001 to 6 August 2002. The dataset comprises some 260 seismograph and accelerograph records, including strong-motion data for seven earthquakes of moment magnitude **M** 4.0 and greater at hypocentral distances less than 10 km.

The temporary Burakin deployment comprised a combination of triaxial short-period seismographs and accelerographs located at a range of distances from near the earthquake epicentres, out to approximately 160 km. In addition to the temporary network, data were also obtained from four government funded, permanent Joint Urban Monitoring Program (JUMP) strong-motion sites located in and around Perth. Sites located in Perth are approximately 190 km from the Burakin sources. All data were recorded at a sample rate of either 100 or 200 Hz and band pass filtered between 0.5 and 30 Hz. No data from Geoscience Australia's National Seismograph Network (ANSN) were used in the present analyses.

All of the earthquakes in the swarm had focal depths less than 2.5 km. Because of the shallow depths, several sites indicated strong radially propagating Rg-phase components. The amplitude of this phase was observed to be highly dependent on focal depth, with the shallowest events indicating the highest degree of Rg-phase contamination. To minimise surface effects from this phase, waveforms were rotated in the horizontal plane to obtain the transverse-component. Windowed transverse shear-waves were used for all subsequent Fourier source and path analyses.

REGRESSION METHODOLOGY:

Analysis of the present dataset largely follows the methods adopted by Atkinson (2004). Fourier amplitude spectra are fitted for 15 discrete frequencies between $0.79 \leq f \leq 19.95$ Hz following an equation of the general form

$$\log A_{ij} = c_1 + c_2 (M - 4) + c_3 (M - 4)^2 - b \log R_{ij} - c_4 R_{ij}, \tag{1}$$

where A_{ij} is the predicted spectral amplitude at site j for event i, R_{ij} is hypocentral distance, b is the geometrical spreading coefficient (i.e. R_{ij}^{-b}), and c_1 through c_4 are parameters to be determined (Atkinson, 2004). Ideally, M is moment magnitude $\mathbf{M}$, however it can be any measure of magnitude provided that both the magnitude type used in the regression and in the prediction of ground-motion are internally consistent.

The anelastic attenuation coefficient c_4, is inversely related to the *seismic quality factor*, Q following

$$c_4 = (\pi f) / [\ln (10) Q \beta], \tag{2}$$

where β (= 3.6 km s^{-1}) is the shear-wave velocity.

Atkinson (2004) states that the geometrical spreading coefficient b is a function of the source-receiver distance. This is largely due to the arrival of other phases within the shear window, corresponding with postcritical reflections from the mid-crustal and Moho discontinuities and Lg-wave arrivals. Consequently, Atkinson (2004) suggests that geometrical spreading in ENA can be described by a hinged trilinear attenuation model.

Once corrected for geometrical spreading and anelastic attenuation, spectral amplitudes can be regressed for quadratic coefficients c_1, c_2 and c_3 to define an empirical spectral attenuation model dependent on magnitude. In the present study, we regress against magnitude $\mathbf{M}$ as calculated by Allen *et al.* (in prep.).

GEOMETRICAL SPREADING:

Since we have a limited number of data to perform regressions in any one magnitude range, Fourier amplitude spectra were normalised to obtain a geometrical spreading model for the Burakin dataset. Windowed shear-wave displacement spectra were calculated and the low-frequency spectral level Ω_{ij} was manually picked for each record. Observed Fourier spectra were smoothed and a series of 22 discrete amplitudes $A_{ij}(f)$, logarithmically distributed from 0.78 to 25 Hz were extracted from each record.

Given the paucity and spatially clustered nature of the Burakin dataset, low-frequency spectral levels are source-corrected for sites with a hypocentral distance of $10 \leq R_{ij} \leq 105$ km. We assume that low-frequency source spectra ($f \leq 2.3$ Hz) can be estimated for all records in this distance range by multiplying by a geometrical spreading coefficient R_{ij} (Atkinson, 2004). Sites within 10 km of the source were ignored in the regression since their spectral amplitudes are susceptible to near-field saturation and radiation pattern effects, coupled with uncertainties in location. The normalising factor Ωn_i for the ith event is defined by averaging Ω_{ij} over the valid hypocentral distance range

$$\log \Omega n_i = \left(1/N_i\right) \sum_{j=1}^{N_i} \left[\log \Omega_{ij} + \log R_{ij}\right] \quad \text{for all } j, \ 10 \leq R_{ij} \leq 105 \text{ km.} \tag{3}$$

N_i is the number of stations that satisfy the hypocentral distance criterion stated above. This procedure is performed assuming that low frequencies are relatively unaffected by anelastic attenuation and scattering at short source-receiver distances ($R_{ij} \leq 105$ km). Each site j over all R_{ij} are subsequently normalised following

$$\log An_{ij}\left(f\right) = \log A_{ij}\left(f\right) - \log \Omega n_i, \tag{4}$$

where An_{ij} is the normalised spectral amplitude for earthquake i at the jth site. This method assumes that the logarithm of normalised spectral amplitude is equal to zero at $R = 1$ km. If we assume Ω_{ij} can be approximated by $A_{ij}(1.5 \leq f \leq 2.3$ Hz), horizontal-component Fourier spectral amplitudes for $10 \leq R_{ij} \leq 105$ km appear to decay as approximately $R^{-1.05}$. Geometrical spreading coefficients with gradients steeper than -1 have also been empirically observed for sites $R \leq 70$ km in ENA (Atkinson, 2004). For sites less than 10 km, normalised spectral amplitudes for the Burakin dataset appear to plateau near the source. Unfortunately, the short hypocentral distance range ($R < 200$ km), coupled with the limited number and spatially clustered nature of the dataset, make it difficult to quantify a hinged geometrical spreading function similar to that of Atkinson (2004). In subsequent analyses, we assume a geometric spreading coefficient $G(R)$ following

$$\log G\left(R_{ij}\right) = \begin{cases} 1.06 \ \log R_{ij} & R_{ij} \leq R_0 \\ 1.06 \ \log R_0 + 0.5 \ \log\left(R_{ij}/R_0\right) & R_{ij} > R_0 \end{cases}, \tag{5}$$

where R_0 is taken to be 80 km; the approximate distance where geometrical spreading becomes less severe owing to surface-wave arrivals from shallow events. R_0 is merely an approximation based on prior studies (e.g. Atkinson, 2004). This relation is employed for subsequent calculations of earthquake source parameters (Allen *et al.*, in prep.).

ANELASTIC ATTENUATION:

In addition to effects from the Rg-phase, strong resonance peaks in the 6-10 Hz band corrupted observed spectra at many of the sites within a hypocentral distance range of 7 to 20 km despite all instruments being located on hard-rock. This phenomenon further complicated attempts to resolve the frequency-dependent quality factor, $Q(f)$. To avoid

these problems, we only use horizontally-rotated, transverse-component data that appear to be relatively unaffected by site effects and complex phase arrivals. This limited the number of data we were able to use to estimate anelastic attenuation and may have introduced azimuthal, distance and instrument dependent biases into our calculations.

The quality factor typically follows the frequency-dependent power law $Q(f) = Q_0 f^\eta$, where Q_0 is the intrinsic quality factor at 1 Hz and η is a numerical constant. The two-station spectral ratio method (Kvamme and Havskov, 1989) was subsequently applied to our data. For frequencies $1.1 \leq f \leq 12.7$ Hz, regression analysis yields the frequency-dependence

$$Q(f) = 290 f^{1.09}.$$

(6)

The horizontal-component intrinsic quality factor in equation (6) is relatively low compared to other stable continental regions [e.g. $Q_0 = 893$ for ENA (Atkinson, 2004)], however, the large frequency exponent in equation (6) gives rise to large values of Q at higher frequencies. The value of Q_0 is slightly higher than crustal values identified by Bowman and Kennett (1991) for central Australia of $Q_0 = 230$.

EARTHQUAKE SOURCE PARAMETERS:

Allen *et al.* (in prep.) calculate moment magnitudes for the Burakin dataset employing the empirical relation of Hanks and Kanamori (1979): $\mathbf{M} = 2/3 \log M_0 - 6.03$, where M_0 is the seismic moment measured in N-m. Magnitudes for the present dataset range between $2.3 \leq \mathbf{M} \leq 4.6$ and demonstrate an M_0-M_L relationship following

$$\log M_0 = 1.14 M_L + 10.45.$$

(7)

Local magnitudes M_L were calculated using the relation of Gaull and Gregson (1991). Further spectral analysis of the Burakin dataset indicates that the average corner frequencies for these events do not vary significantly with M_0, chiefly ranging between 2-3 Hz (Allen *et al.*, in prep.) for events $\mathbf{M} > 3.0$. This gives rise to relatively low stress drops for the lower magnitudes ($\mathbf{M} < 4.0$) that increase at larger magnitudes. Average stress drops for the larger magnitude events ($\mathbf{M} > 4.0$) appear to be relatively high (approximately 10 MPa) and are consistent with values obtained from southeastern Australian earthquakes (Allen *et al.*, in press).

RESULTS AND DATA ANALYSIS:

Table 1 provides regression coefficients for the fit of horizontal-component spectral amplitudes. Predicted Fourier acceleration spectral amplitudes for earthquakes of magnitude $2.3 \leq \mathbf{M} \leq 4.6$ based on these coefficients can be written as

$$\log A_{ij} = c_1 + c_2 (\mathbf{M}_i - 4) + c_3 (\mathbf{M}_i - 4)^2$$
$$-1.05 \log R_{ij} - c_4 R_{ij} \qquad \text{for } R_{ij} \leq 80 \text{ km}$$

(8a)

$$\log A_{ij} = c_1 + c_2 (\mathbf{M}_i - 4) + c_3 (\mathbf{M}_i - 4)^2$$
$$-1.05 \log(80) - 0.5 \log(R_{ij}/80) - c_4 R_{ij} \quad \text{for } R_{ij} > 80 \text{ km}$$

(8b)

Frequency (Hz)	c_1	c_2	c_3	c_4	Q
0.79	1.169	1.529	0.0757	0.00133	226
1.00	1.341	1.526	0.0272	0.00131	290
1.26	1.534	1.464	-0.0240	0.00128	373
1.58	1.666	1.389	-0.0558	0.00125	479
2.00	1.768	1.295	-0.0783	0.00123	616
2.51	1.815	1.252	-0.0828	0.00120	791
3.16	1.853	1.224	-0.0777	0.00118	1017
3.98	1.860	1.199	-0.0656	0.00115	1307
5.01	1.840	1.152	-0.0549	0.00113	1680
6.31	1.806	1.069	-0.0480	0.00111	2160
7.94	1.767	1.001	-0.0421	0.00108	2776
10.00	1.757	0.945	-0.0330	0.00106	3568
12.59	1.748	0.897	-0.0153	0.00104	4586
15.85	1.704	0.882	0.0117	0.00102	5894
19.95	1.616	0.850	0.0456	0.00100	7575

Table 1. Coefficients of regression for horizontal-component Fourier amplitudes for Burakin, WA, earthquakes of magnitude $2.3 \leq M \leq 4.6$ [equation (8)].

Values describe Fourier acceleration spectra in mm s^{-1}.

Figure 1 compares some observed spectra (for two magnitude and distance ranges) with the predicted spectral amplitudes of this study and with Atkinson's (2004) model derived for ENA. Modelled spectral amplitudes are calculated at the mid-point of the distance range. Predicted amplitudes are plotted using the upper and lower magnitude limits. In general, our empirical attenuation model fits the observed data quite well. Outliers will be expected since the model is an average representation of observed ground-motion. The WA model appears to predict higher Fourier amplitudes at low frequencies than Atkinson (2004), particularly at short source-receiver distances. The disparity between the two models at low frequencies most likely arises from issues concerning differences in geometrical spreading. The magnitude scales used for each study appear to be consistent since the low-frequency level ($f < 2$ Hz) of the source spectrum (i.e. at $R = 1$ km) is equivalent for both models[1].

Residuals of modelled WA ground-motions are plotted against hypocentral distance (Figure 2). Residuals at sites j are defined as the logarithm of predicted spectral amplitudes, less the logarithm of observed spectra for an event of magnitude M_i at R_{ij} km. Modelled spectra appear to slightly overestimate observed horizontal-component ground-motions between 10-20 km at 1 Hz, however, residuals at greater distances are generally quite low.

CONCLUSIONS:

Regression analysis of Fourier spectra indicates that the decay of spectral amplitudes can be approximated by a geometrical spreading coefficient of $R^{-1.05}$ within 80 km of the source. Beyond 80 km, we use theoretical cylindrical spreading of $R^{-0.5}$ (Herrmann and Kijko, 1983). The associated model for the regional seismic quality factor can be expressed as $Q(f) = 290 f^{1.03}$

---

[1] Note: we convert M for modelled spectra to m_1 using equation (12) in Atkinson (2004) and substitute into the ENA ground-motion model (Figure 1.).
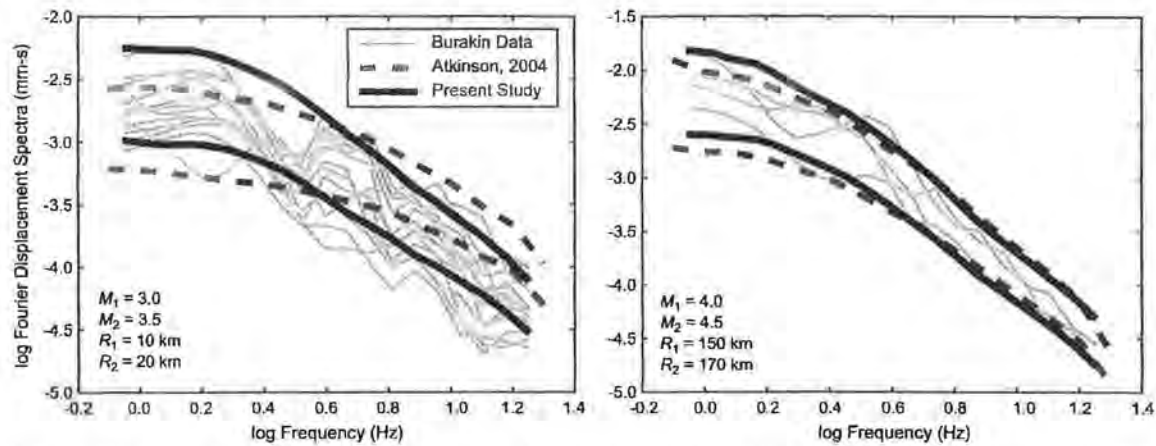
Figure 1. Comparison of Fourier Displacement Spectra derived from the Atkinson (2004) attenuation model and the present study. The two sets of heavier lines in each plot indicate the bounds of the maximum and minimum magnitudes (M_1 and M_2) calculated at the mid-distance of the data range (R_1 and R_2). Thin lines represent observed spectra recorded within the prescribed magnitude and distance range.
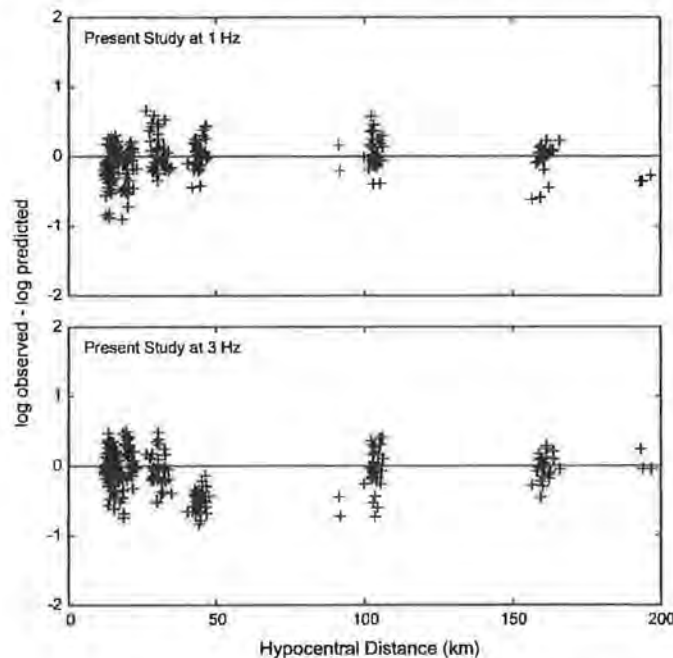

Figure 2. Residuals of modelled WA ground-motions plotted against hypocentral distance. Note that the site at approximately 45 km indicated anomalous frequency decay beyond 2 Hz. Consequently no data from this site were used in the regression of the ground motion model indicated in Table 1. Similarly, sites at $R > 190$ km were located in the geologically dissimilar Perth Basin and were not considered suitable to be included in the regressions either.

Using the coefficients derived in Table 1, modelled horizontal-component displacement spectra appear to fit the observed data very well. Spectral amplitude residuals are on average, relatively small and do not appear to vary significantly with hypocentral distance. Given the narrow magnitude range of the data ($2.3 \leq M \leq 4.6$), **we cannot be certain of the model's behaviour if extrapolated to larger magnitudes**. Furthermore, since the Burakin dataset comprise an earthquake swarm, results of Allen *et al.* (in prep.) suggest that all but the largest of these swarm events appear to have anomalously low corner frequencies and stress drop. We are therefore concerned that an attenuation model based on such events may have limited application for predicting ground-motions of isolated crustal events. This gives added impetus for the need to include more data in our work and to expand this research into different seismotectonic regions within the Australian continent.

This preliminary work provides an important framework for developing regional ground-motion relations in Australia. Attenuation parameters derived in these empirical studies are used as key inputs for stochastic models to predict ground-motions for larger magnitude events.

ACKNOWLEDGEMENTS:

REFERENCES:

Allen, T.I., Cummins, P., Dhu, T., Leonard, M. and Schneider, J.F. (in prep.). Low stress drop swarm events in the Yilgarn Craton, Western Australia.

Allen, T.I., Gibson, G., Brown, A. and Cull, J.P. (in press). Depth variation of seismic source scaling relations; Implications for earthquake hazard in southeastern Australia. Tectonophys.

Atkinson, G.M. (2004). Empirical attenuation of ground-motion spectral amplitudes in southeastern Canada and the northeastern United States. Bull. Seism. Soc. Am., Vol 94, pp 1079-1095.

Atkinson, G.M., and Boore, D.M. (1995). New ground motion relations for eastern North America. Bull. Seism. Soc. Am., Vol 85, pp 17-30.

Bowman, J.R. and Kennett, B.L.N. (1991). Propagation of *Lg* waves in the North Australian Craton: Influence of crustal velocity gradients. Bull. Seism. Soc. Am., Vol 81, pp 592-610.

Dhu, T. and T. Jones (Eds., 2002). Earthquake risk in Newcastle and Lake Macquarie, Geoscience Australia Record 2002/15, Geoscience Australia, Canberra.

Gaull, B.A. and Gregson, P.J. (1991). A new local magnitude scale for Western Australian earthquakes. Aust. J. Earth. Sci., Vol 38, pp 251-260.

Hanks, T.C. and Kanamori, H. (1979). A moment magnitude scale. J. Geophys. Res., Vol 84, pp 2348-2350.

Herrmann, R.B. and Kijko, A. (1983). Modeling some empirical vertical component Lg relations, Bull. Seism. Soc. Am., Vol 73, pp 157-171.

Kvamme, L.B. and Havskov, J. (1989). Q in southern Norway. Bull. Seism. Soc. Am., Vol 79, pp 1575-1588.

Leonard, M. (2003). Respite leaves Burakin quaking in anticipation. AUSGEO News, Vol 70, pp 5-7.

Robinson, D., Dhu, T. and Schneider, J.F. (2004). The effect of different attenuation models on earthquake hazard in the Newcastle and Lake Macquarie region, Australia. *Proc. ASEG-PESA 2004 Conference*, Sydney.

Toro, G.R., Abrahamson, N.A. and Schneider, J.F. (1997). Engineering model of strong ground motions from earthquakes in the Central and Eastern United States. Seism. Res. Lett., Vol 68, pp 41-57.

A SOIL RESPONSE SPECTRUM MODEL FOR MELBOURNE

SRIKANTH VENKATESAN[1], NELSON LAM[1], JOHN WILSON[1] AND MICHAEL ASTEN[2]

1. Department of Civil & Environmental Engineering, University of Melbourne, Victoria, Australia.
2. Centre for Environmental and Geotechnical Applications of Surface Waves (CEGAS), School of Geosciences, Monash University, Melbourne, Victoria, Australia.

AUTHORS:

Srikanth Venkatesan is a PhD student at University of Melbourne, Melbourne.

Nelson Lam is a Senior Lecturer at University of Melbourne, Melbourne.

John Wilson is an Associate Professor at University of Melbourne, Melbourne.

Michael Asten is a Professorial Fellow at Monash University part-time and is also a consulting geophysicist and Partner with Flagstaff Geo-Consultants, Melbourne.

ABSTRACT:

A new model used in constructing response spectra representing conditions pertaining to resonance on soft soil sites is presented in this paper. Factors controlling the extent of soil amplifications including the shape of the soil shear wave velocity profile, hysteretic damping properties of the soil and impedance contrast between soil and bedrock have been taken into account in the model. The last of these factors controls the extent of radiation damping which is highly dependent on the shear wave velocity of the bedrock close to its interface with soil sediments. The prediction for this radiation damping factor has been filled with uncertainty since information related directly to the strength and stiffness of the bedrock is not included in a typical borehole record. The shear wave profiling in Silurian mudstone in the Melbourne area using the SPAC (Spatial Auto-Correlation) method as reported in a companion paper fills this important gap. This shear wave velocity information newly obtained for the Melbourne area has been incorporated into the seismic soil amplification model presented in this paper.

1. INTRODUCTION

Engineering codes of practice typically classify local soil conditions into discrete site classes based on the average shear wave velocity (SWV) of the soil in the upper layers. The International Building Code IBC(2000) for example, recommends amplification factors that are functions of the site class and the level of seismic hazard. Soil amplification is highly dependent on the impedance contrast at the rock-soil interface (which controls the amount of radiation damping), the soil shear wave velocity gradient and the soil hysteretic properties. Code provisions for high seismic regions such as IBC(2000) do not explicitly parameterise these effects individually. Such code provisions have been based on regression analyses of instrumented strong-motion data that has been augmented by analytical results (Dobry, 2000). Regions like Australia that do not have sufficient strong motion data would typically adopt provisions developed originally in well studied data-rich regions like Western North America. Note, the majority of structures in Australia are non-ductile and hence have relatively little energy dissipation capacity. Consequently, structures experiencing earthquake excitations in these regions will be particularly sensitive to the soil response behavior pertaining to resonance conditions. Importantly, the extent of soil amplification is controlled by the SWV of the bedrock governing the impedance. In practice, bedrock SWV is not measured in normal engineering site investigations. Thus there are great uncertainties in the modeling of the soil amplification effects in practice. The companion papers presented in this conference, [Roberts et al., 2004 and Lam et al., 2004] describes the application of a new technique known as SPAC (a passive seismological monitoring technique based on the analyses of surface waves), in measuring and modelling the SWV profile in bedrock. Of particular interest in this paper is the incorporation of such information in quantifying the effects of radiation damping, which in turn controls the overall level of soil amplification.

This paper introduces a new model for estimating the extent of soil amplification based on the aforementioned modelling considerations. The soil amplification factor defined in Figure 1, is represented by its component factors and is expressed in the form

$$S = S_\psi \, S_\xi \, S_\lambda \tag{1}$$

The definition of amplification factor in Figure 1 was first introduced in Lam et al., (2001). The first factor S_ψ represents the effects of the shape of the soil shear wave velocity profile. S_ξ represents the effects of hysteretic damping and S_λ represents the effects of radiation damping. Both S_ψ and S_λ have been normalized to unity. Each of these factors is addressed in sections 2 – 4. The developed model as a whole is then summarized in Section 5 with concluding remarks in Section 6.

Nine soil profiles from Melbourne having natural periods in the range 0.35 - 0.95 s have been analysed. These sites fall in the category of Site class C or D according to IBC 2000 & AS 1170.4 (2004). Program SHAKE-91 [Schnabel et-al, 1972] computes quasi non-linear response of soil profiles based on one-dimensional shear wave analyses of soil columns is adopted in this study. The use of this methodology for soil response analyses is well supported in the literature [Dickenson 1991, Seed 1994, Dobry 2000]. Bedrock accelerograms for magnitude 7 have been simulated using program GENQKE [Lam, 2000].
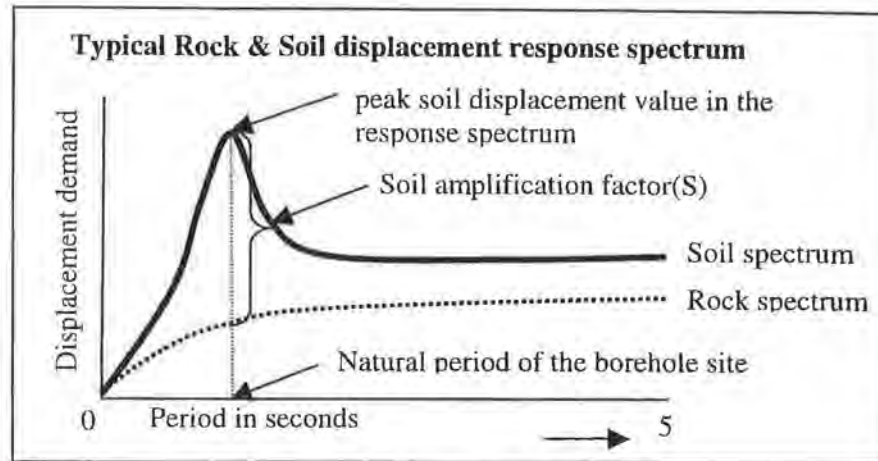
Figure 1. Definition of Soil Amplification factor

2. Soil SWV Profile factor S_ψ

To investigate the effects of the soil shear wave velocity profile, the selected sites were grouped into irregular, linear and polynomial profiles as shown in Figure 2 (depth range 15 - 55m). The factors listed for each profile type were obtained from comparative analysis using SHAKE-91. It is recognized that not all soil profiles can be distinctly classified as linear or polynomial profiles and soil profiles may exhibit a complex combination of different profiles. Studies are continuing to determine the extent in which these factors can be applied in practice. Notwithstanding this, Figure 2 provides very useful indications on the sensitivity of soil amplification to the shape of soil SWV profile.

Soil SWV Profile	Weighted average uniform profile (reference profile)	Irregular profile	Linear profile	Polynomial profile
S_ψ	1	1.3	1.4	1.5

Figure 2. Effects of Soil Shear wave velocity profiles on Soil Amplification factors

3. Hysteretic Damping factor S_ξ

Trends related to the effects hysteretic damping were studied by varying the intensity of the input motion at bedrock level with Peak Ground Velocity (PGV) varying between 20 and 100 mm/sec. Soil sites have been idealized to possess constant Plasticity Index (PI). It is noted that a real soil profile typically contains a combination of materials with different PI. Notwithstanding this, Figure 3 provides useful indications on the sensitivity of soil amplification behavior on the hysteretic properties of the soil.
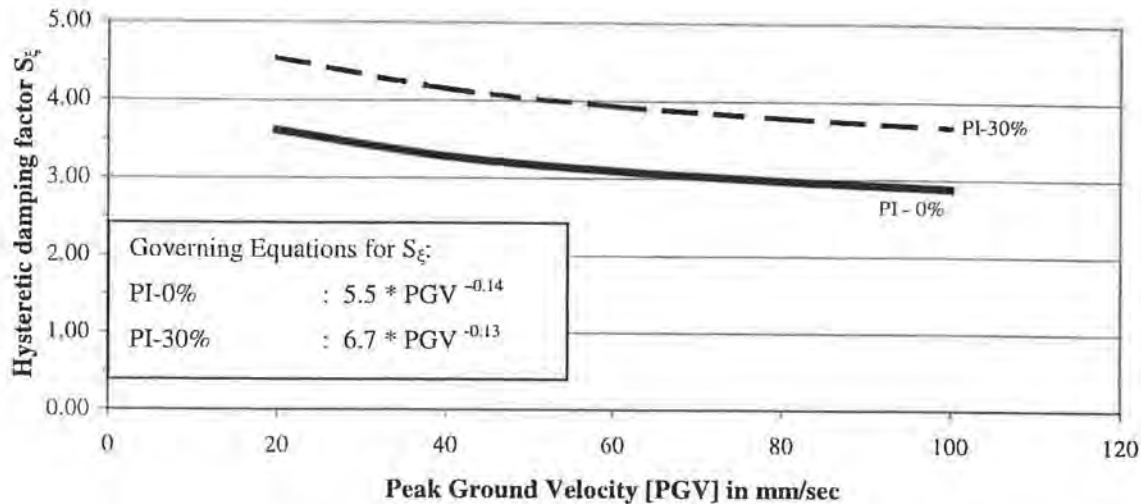
Figure 3. Influence of soil material type and PGV on hysteretic damping

It is shown in Figure 3 that the sensitivity of the S_ξ factor on PGV is variable. For any given site with a random combination of different material types, the actual S_ξ curve would be some weighed average of the idealized curves shown in the figure. (Since the soil profiles considered in this study were composed of PI-0 & PI-30, only these curves have been presented) The soil dynamic properties pertinent to the analyses are presented in Appendix A. Governing equations for S_ξ presented in Figure 3 have been evaluated by residual analyses the results of which are presented in Figure 4.
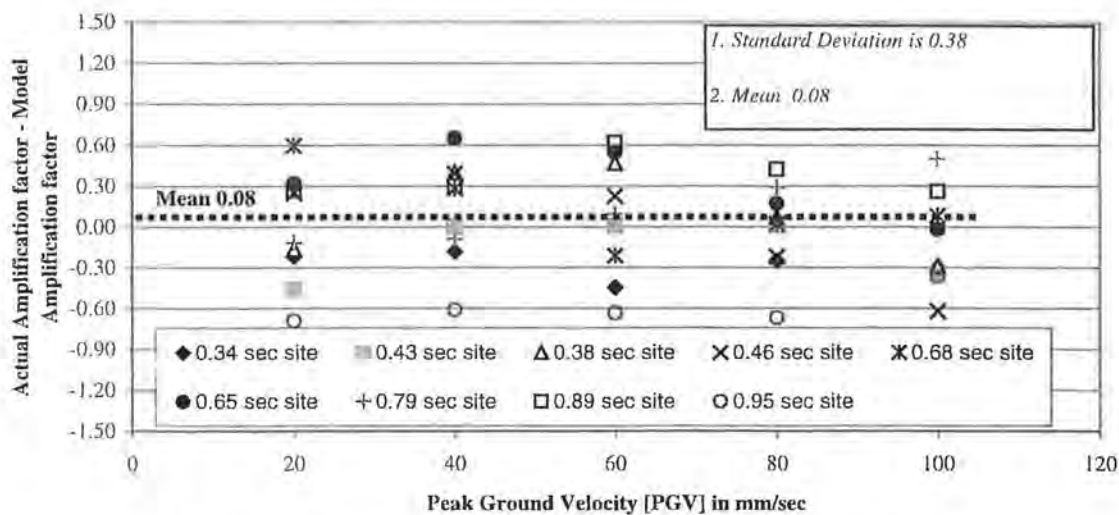

Figure 4. Residual analyses of hysteretic damping factor S_ξ
[based on equations in Figure 3]

It is noted from Figure 4 that the residual analysis shows no significant bias in the model in view of the closeness of the mean of the residuals to zero.

4. Radiation Damping factor S_λ

As noted earlier, the radiation damping factor has been normalized to unity at reference bedrock SWV of 1000 m/sec. Factors associated with other half-space SWV values are presented in Table 1.

Bedrock SWV in m/sec	Radiation damping factor S_λ
1000 m/sec	1
1500 m/sec	1.125
2000 m/sec	1.25

Table 1. Radiation Damping factor S_λ

The above factors are based on rock SWV values representing a half-space. It is noted that in reality the bedrock is far from being a half-space with uniform SWV profile. An equivalent bedrock half-space that would have similar amplification properties as that of actual bedrock would need to be identified. A 1 sec soil site was analysed with the rock SWV profiles represented down to a depth of 500 m. The corresponding input motions at 500 m depth and that at rock outcrop were generated using program GENQKE. The SWV value of the idealised half-space was calibrated to achieve a match in the computed values for RSV$_{max}$ as shown in Figure 5. The half-space SWV was found to correspond to an effective depth of 100 m into bedrock. Sheikh (2003) conducted a similar calibration for Hong Kong conditions and identified an effective depth of only 30 m.
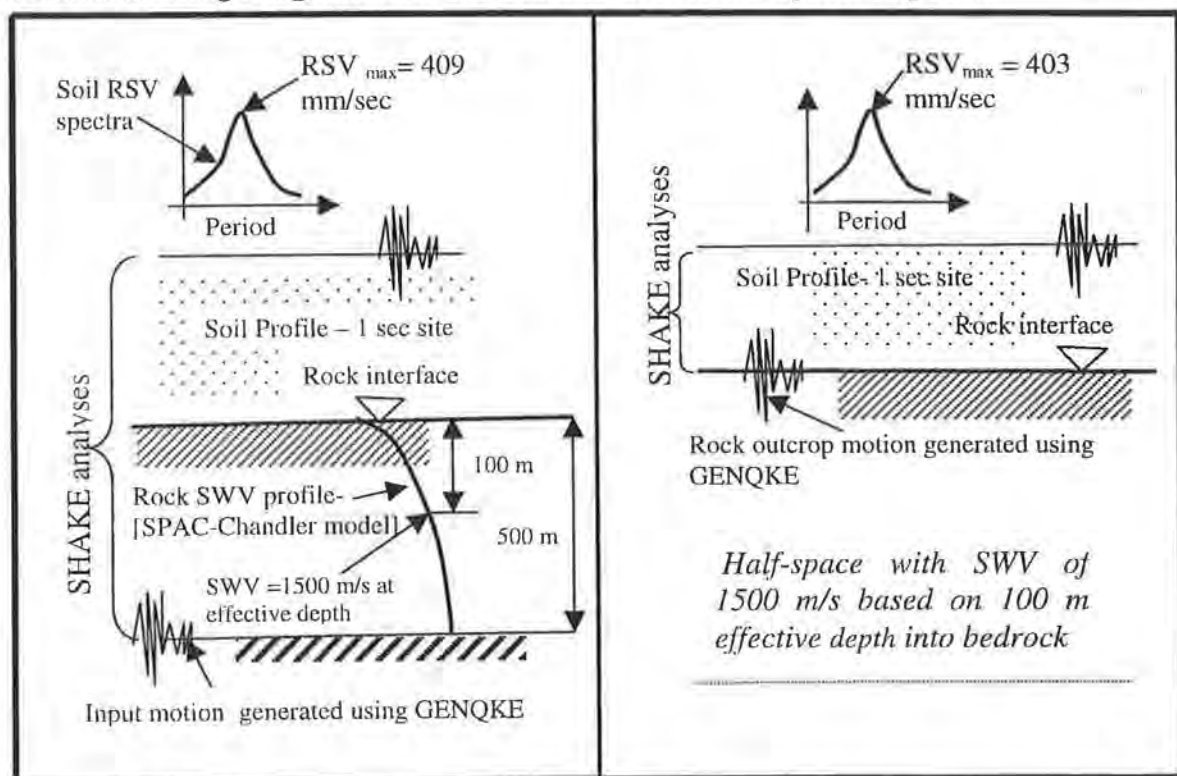

Figure 5. Equivalent bedrock half-space SWV value for Melbourne conditions

5. SUMMARY OF THE PROPOSED MODEL

The component soil amplification factors introduced and developed in this paper are summarized herein in the form of simple algebraic relationships:

S_ψ = 1 for soils possessing a uniform shear wave velocity profile (reference case)

= 1.3 for soils possessing an irregular shear wave velocity profile (typical soil profile in practice)

= 1.4 for soils possessing a distinct linear shear wave velocity profile

= 1.5 for soils possessing a distinct polynomial shear wave velocity profile

S_ξ for different soil material types (categorized by PI value) is given by

$S_\xi = 3.9 * PGV^{-0.14}$, (for PI-0%)

$S_\xi = 4.8 * PGV^{-0.13}$, (for PI-30%)

$S_\lambda = 1 + 0.00025 (V_{bedrock} - 1000)$ and $0.9 \leq S_\lambda \leq 1.25$ (where $V_{bedrock}$ is bedrock SWV in m/sec)

6. CLOSING REMARKS

A new model for estimating the soil amplification factor in intra-plate conditions pertaining to resonance on soft soil conditions has been presented. The model is based on component factors representing various observed phenomenon in soil amplification. Simple expressions have been developed to represent the effects of the soil shear wave velocity profiles, hysteretic and radiation damping properties. Importantly, radiation damping is highly dependant on the SWV properties in bedrock governing the impedance. In principle this crucial information is available with the newly developed SPAC technique, although limitations in array sizes used to date yield inadequate resolution of the basement SWV [Roberts et al., 2004, this volume]. Standard deviation and mean of the residual amplification factors have been computed to evaluate the developed model. It is recognized that the amplification factors derived from the proposed model would generally be higher by about 1.5 times, than the code provisions of IBC 2000 and AS 1170.4 (1993 & 2004), since code provisions are based on averaging across a range of soil conditions.

7. REFERENCES

Australian Standard - AS 1170.4, (1993) Minimum design loads on structures, Part 4: Earthquake loads, Standards Association of Australia, North Sydney, NSW, Australia

Australian Standard - AS 1170.4, (2004) Structural Design Actions : Earthquake Actions in Australia, Pre-Public comment draft, 5212-PDR-311, Feb, 2004.

Dickenson, S.E., Seed, R.B., Lysmer, J., and Cok, C.M., (1991) Response of soft soils during the 1989 Loma Preita earthquake and implications for seismic design criteria, Proceedings of the Pacific conference on earthquake engineering, New Zealand, pp 191-203.

Dobry, R., Borcherdt, R.D., Crouse, C.B., Idriss, I.M., Joyner, W.B., Martin, G.R., Power, M.S., Rinne, E.E., and Seed, R.B., (2000) New site coefficients and site classification system used in recent building seismic code provisions, Earthquake Spectra, Vol 16, No 1, pp 41-67.

Hardin, B.O., and Drnevich, V.P., (1972) Shear modulus and damping in soils: Measurement and parameter effects, Journal of Soil Mechanics and Foundations, American Society of Civil Engineers, Vol 98 (SM6), pp 603-624.

International Building Code – IBC 2000, (2000) International Code Council (ICC), USA.

Lam, N.T.K., Wilson, J.L., (1999) Estimation of the site natural period from borehole records, Australian Journal of Structural Engineering, Vol SE1 (3) pp 179-199

Lam, N.T.K., Wilson, J.L., and Hutchinson, G.L., (2000) Generation of synthetic earthquake accelerograms using seismological modeling: a review, Journal of Earthquake Engineering, Vol 4, No 3, pp 321-354.

Lam, N.T.K., Wilson, J.L., and Chandler, A.M., (2001) Seismic displacement response spectrum estimated from the frame analogy soil amplification model, Journal of Engineering Structures, Vol 23 (11), pp 1437-1452.

Lam, N.T.K., Asten, M., Chandler, A.M., Tsang, H., Venkatesan, S. and Wilson, J., (2004) Seismic attenuation modelling for Melbourne based on the SPAC-CAM procedure, Proceedings of the Conference of Australian Earthquake Engineering Soc., Mount Gambier, [this volume].

Roberts, J., Asten, M., Tsang, H., Venkatesan, S. and Lam, N.T.K., (2004) Shear wave velocity profiling in Silurian mud stone using the SPAC method, Proceedings of the Conference of Australian Earthquake Engineering Soc., Mount Gambier, [this volume].

Schnabel, P.B., Lysmer, J., and Seed, H.B., (1972) A computer program for earthquake response analysis of horizontally layered sites. Earthquake Engineering Research Centre EERC report 72-12. Berkeley (CA): University of California at Berkeley.

Seed, R.B., Dickenson, S.E., Rau, G.A., White, R.K., and Mok, C.M., (1994) Observations regarding seismic response analyses for soft and deep clay sites, Proceedings of the 1992 NCEER/SEAOC/BSSC Workshop on site response during earthquakes and seismic code provisions, National Centre for Earthquake Engineering Research Special Publication NCEER-94-SP 01, Buffalo, NewYork.

Sheikh, M.N., (2003) Effect of bedrock rigidity on site response study for typical Hong Kong rock classes, Internal report, Department of Civil Engineering, University of Hong Kong., Hong Kong.

Vuectic, M., and Dobry, R., (1991) Effect of soil plasticity on cyclic soil response, Journal of Geotechnical Engineering, American Society of Civil Engineers, Vol 117, pp 89-109

Vuectic, M., Lanzo, G., and Doroudian, M., (1998) Damping at small strains in cyclic simple shear test, Journal of Geotechnical and Environmental Engineering, Vol 124, pp 585-594

8. APPENDIX - A

Summary of Soil Dynamic Properties

Stiffness Degradation [Hardin & Drnevich model, 1972]

$$\frac{G}{G_{max}} = \frac{1}{\left(1 + \frac{\gamma}{\gamma_{ref}}\right)} \qquad\qquad \text{Eqn} \quad (2)$$

Viscous Damping

$$\zeta = \zeta_i + \zeta_{max} \frac{\left(\frac{\gamma}{\gamma_{ref}}\right)}{\left(1 + \frac{\gamma}{\gamma_{ref}}\right)} \qquad\qquad \text{Eqn} \quad (3)$$

$$\zeta_i = 0.015 + 0.0003 \times PI(\%) \le 0.058$$
$$\zeta_{max} = 0.16 - 0.001 \times PI(\%) \ge 0.0$$

where,

G is the dynamic shear modulus

G_{max} is the initial dynamic shear modulus at very low shear strain

γ is the shear strain level in soils typically in the order of 0.0001% to 0.1%

γ_{ref} is the reference strain level identified to match the equations presented in Appendix-A [Lam and Wilson, 1999]

ζ_i is the initial damping at very low shear strain

ζ_{max} is the maximum damping at shear failure.

Table A1. Soil Parameters Summary

Soil Type	PI %	γ_{ref}	ζ_i	ζ_{max}
Sand	0	0.00025	0.015	0.16
Clay	15	0.00045	0.0195	0.145
Clay	30	0.001	0.024	0.13
Clay	50	0.002	0.030	0.11
Clay	100	0.004	0.045	0.06

Note : Higher damping values at initial strain levels may be predicted by the above equations for soil PI-100%, which accommodate the findings of Vuecitc et-al.(1998)

Figure A1 presents a comparison of Modulus reduction curves developed using equations (2) & (3) with the modlulus reduction curves recommended by Vuectic and Dobry (1991).
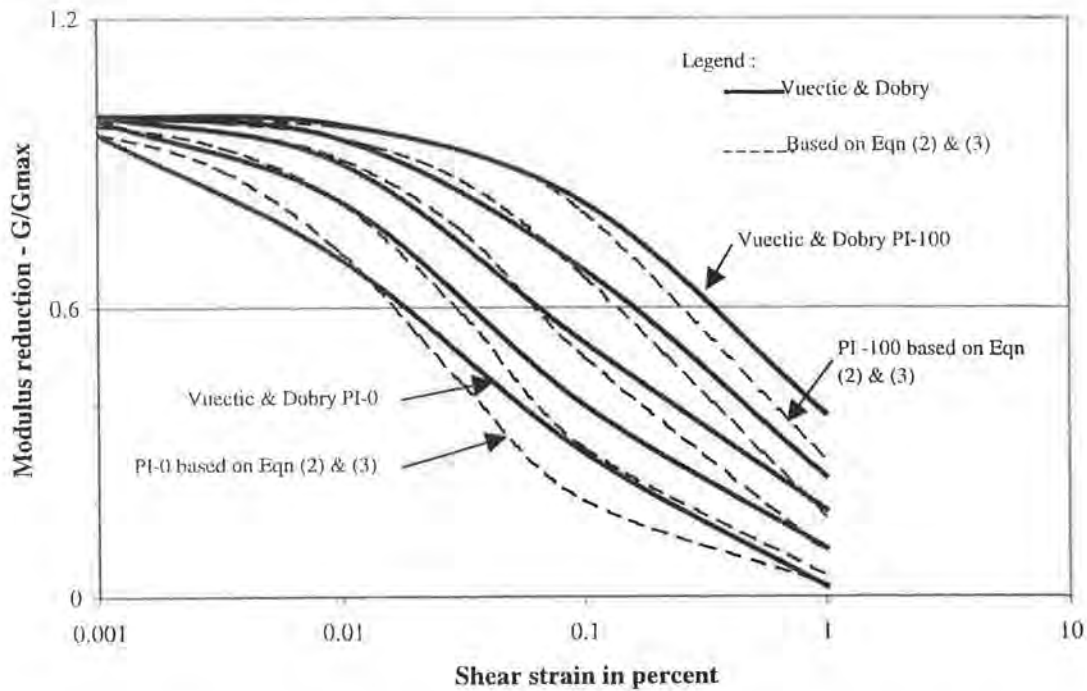

Figure A1. Shear modulus reduction curves – Comparison based on curves calibrated using Eqn (2) & (3) with Vuectic and Dobry (1991) recommendations.

SOFT SITE RESPONSE AT LONG RANGE: THE WAINUIOMATA BASIN

W.R. (Bill) Stephenson,
IGNS, Lower Hutt, New Zealand.

AUTHOR:

Bill Stephenson is a senior scientist with the Institute of Geological and Nuclear Sciences, Lower Hutt, New Zealand. After graduating in 1966 (in physics) from Victoria University in Wellington, Bill entered government service, working for DSIR in the area of strong motion seismology. The 1967 Caracas earthquake initiated his interest in microzoning which he has since pursued, with an emphasis on field measurements. Later, employment in the electronics industry sharpened his instrumentation skills, and a period in soil engineering helped him understand better what is involved in the response of soils to shaking. Bill introduced seismic CPT and the Nakamura method to New Zealand, and is the inventor of the Stephenson Probe, which uses the installation of low-noise silicon accelerometers at depth, by penetrometry. Bill works with Chávez-García and with Lomnitz, both from UNAM, Mexico.
Email: bill.stephenson@gns.cri.nz

ABSTRACT:

For each of two 350km distant earthquakes, the Wainuiomata (Lower Hutt, New Zealand) soft site is shown to respond vigorously at the expected arrival time of waves travelling from the epicentre at 2.7km/sec. A dispersion curve based on the upper-crustal velocity structure indicates that, at the site resonant frequency, Rayleigh waves should travel at this speed. For a closer earthquake, array studies of rock motion confirm that Rayleigh waves of this same speed do traverse the array, with time, propagation direction, and speed all having appropriate values. However for the two distant earthquakes the rock motion at nearby sites has no obvious special character at the arrival time of the Rayleigh waves. It is concluded that arriving Rayleigh waves are particularly efficient at exciting the Wainuiomata site. Late arriving waves which efficiently excite site resonance provide an explanation of long duration shaking and hence of excessive damage for soft sites during distant earthquakes.

SOFT SITE RESPONSE AT LONG RANGE: THE WAINUIOMATA BASIN

W.R. (Bill) Stephenson, Institute of Geological and Nuclear Sciences, Lower Hutt, New Zealand.

1. INTRODUCTION

There are many opinions regarding the role of soft soils during earthquake shaking, covering the range from "soft soils always absorb energy, fail, and isolate vibration" to "soft soils always amplify motion, leading to great damage". Believers in these two end points of the range are unlikely to become reconciled in all respects, but there is apparently a middle ground for which there is agreement – that for large, distant, shallow earthquakes, amplification and long duration shaking are the rule.

Despite this agreement there is no consensus as to the processes involved in determining the extended duration of shaking observed on soft soils during large distant earthquakes. However extended duration of shaking is a crucial aspect of spectral amplification by soft soils, because it allows cumulative damage to occur, implying large increases of damage at relatively low levels of shaking. Beck and Hall (1986) cite the example of damage to buildings founded on soft soil in Mexico City during the 1985 Michoacán earthquake being a result of long duration shaking.

2. POSSIBLE GENERATORS OF LONG DURATION SHAKING

Long duration shaking in a basin can conveniently be divided into two major categories according to whether it originates outside or inside the basin. In the former case it is supposed that multipathing over the long distance from the source gives rise to prolonged shaking on the rock surrounding and underlying a soft site, and that the role of the soft soil is simply to amplify that prolonged motion. This mechanism was advanced in the context of Mexico City by Singh and Ordaz (1993). In the latter case it is supposed that the soil deposit itself somehow prolongs the shaking. One mechanism which could cause prolonged shaking is the local generation and propagation of slow waves within the basin, where the combination of low speed and propagation distance on the soil can give rise to delays. Such waves were evaluated by Chávez-García and Bard (1994).

Both origins of long duration shaking have been challenged. For long durations which originate outside the basin, experimental evidence is lacking, with unrecorded rock motion (as a consequence of level-determined recording) being supposed to result in long duration soil motion. For long durations which originate inside the basin, modelling studies suggest that locally-generated waves will die out before they have travelled a sufficient distance, due to energy loss in the soft soil.

Long duration shaking attributable to locally-generated waves has been observed in the Valley of Mexico (Stephenson, 2002) and this paper will document long duration shaking attributable to late-arriving rock motion at a site in New Zealand.

3. UPPER-CRUSTAL RAYLEIGH WAVE PROPAGATION

Informal inspection of many accelerograms recorded in New Zealand on soft sites and caused by distant earthquakes suggested a common factor – that resonant motion often occurred, consistent with excitation by waves propagating from the epicentre at 2.7km/s. This suspicion could never have greater status than a suggestion for further work because the accelerometer clock timing was never scientifically defensible. However it stimulated an investigation of upper-crustal Rayleigh wave propagation (as being a likely candidate). Because many of the instances of late excitation of resonant motion were associated with the Wainuiomata site near Wellington, this site has become central to the investigations. At Wainuiomata, 31m of ex-lake fine-grained sediments give rise to resonant responses between 0.8Hz and 1.2Hz. The frequency indicated using the method of Nakamura (1989) is 0.8Hz. The Wainuiomata site is described by Begg *et al* (1993).

Contemporary views of the crustal structure in New Zealand reject the traditional notion of several horizontal layers, and instead adopt a three-dimensional structure. However up until recently a layered structure was successfully used to explain seismic arrivals, and to minimise the residual errors in these arrivals, and such a structure provides a starting point to evaluate Rayleigh wave propagation. Figure 1 shows the structure adopted for central New Zealand, and the associated fundamental Rayleigh wave dispersion curve. Note that near 1Hz (the Wainuiomata site frequency is 0.8Hz) a group velocity near 2.7km/s is predicted.
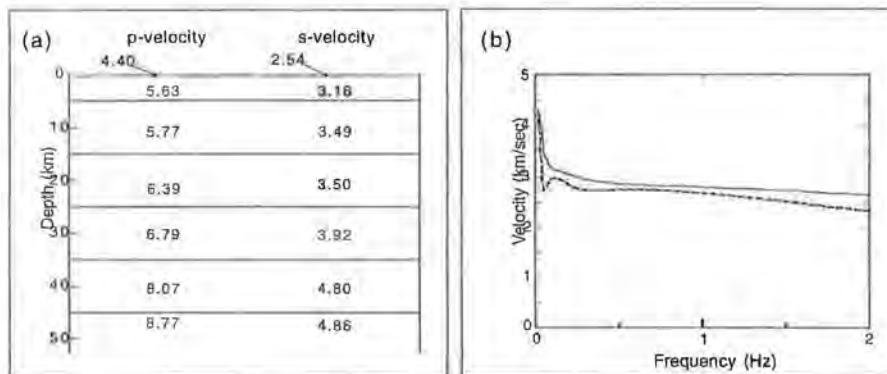

Figure 1. (a) Crustal structure assumed for central New Zealand. (b) Dispersion curve for fundamental mode Rayleigh waves based on the assumed crustal structure. Solid line is phase velocity and dotted line is group velocity.

4. RAYLEIGH WAVE IDENTIFICATION

Given the uncertain nature of the crustal structure upon which the previous dispersion curves were based, it is pertinent to see whether the predicted Rayleigh waves can be identified in field measurements using rock near the Wainuiomata site. To this end, the results of a 1995 deployment of an array of 3-component velocity seismometers are useful. The 1995 Parkway array included four rock-based stations arranged in a quadrilateral with sides of roughly 400m. See Chávez-García *et al* (1999).

A well-recorded earthquake of magnitude 4.9 which occurred 81km away from the Parkway array, at 21km depth, provides an opportunity to look for Rayleigh waves with a velocity of 2.7km/sec. An accurate value for source time, plus accurate timing on the seismographs, allows the expected window for 2.7km/sec waves (30 seconds after source time) to be selected and examined. For this window the wavenumber spectrum and the particle orbit shown in figure 2, for a frequency band centred around 1Hz, both confirm Rayleigh wave motion.
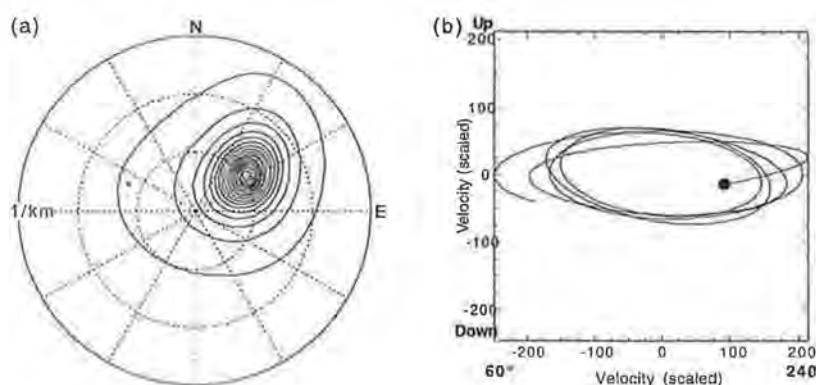

Figure 2. (a) Wavenumber spectrum for the 60 degree component of motion between 0.9Hz and 1.1Hz, at 30sec to 35sec after source time, showing a wave travelling in the direction 240 degrees at 2.7km/sec. (b) Particle orbit for the same time and frequency windows in the 240deg/vertical plane, with a dot showing the start. Together, (a) and (b) show a Rayleigh wave travelling from the epicentre.

A wavenumber spectrum is the spatial equivalent of a frequency spectrum and its peak indicates the direction and wavenumber (inverse of wavelength) of incoming waves, from which their velocity can be determined. The particle orbits are retrograde elliptical as expected for fundamental mode Rayleigh waves on the surface of a half-space. The velocity for the time window is consistent with Rayleigh waves travelling from the epicentre.

5.   LATE RESONANCE AT THE WAINUIOMATA SITE

As was mentioned earlier, high quality records of shaking on soft soil due to distant earthquakes are relatively rare. In part this deficiency is a consequence of a late realisation that good strong-motion timing is important, but it is exacerbated by a lack of large earthquakes and by difficulties in an accelerograph identifying earthquake shaking on soft soil and then triggering a recording. Both these drawbacks are vanishing because newer recorders have GPS-based clocks, and enough memory to allow continuous recording.

Even though the Wainuiomata accelerogram of the magnitude 6.6 Arthurs Pass earthquake of 18 June 1994 has unreliable absolute timing, it is tractable because a plausible route exists for determining that timing. In essence the route involves identifying a long-period wave in the double-integrated accelerogram, and the same

wave on a seismograph 20km distant, which has an accurate clock. This allows timing to be established to within a few seconds, and this timing can then be refined by associating initial triggering with the arrival of the Sg phase on the accelerogram. A detailed description of the procedure will be published elsewhere. As shown in figure 3 the second triggering, which is associated with a major episode of resonant motion, is at the expected arrival time of waves travelling at 2.7km/s (which is indicated by the letter "R" in the figure).
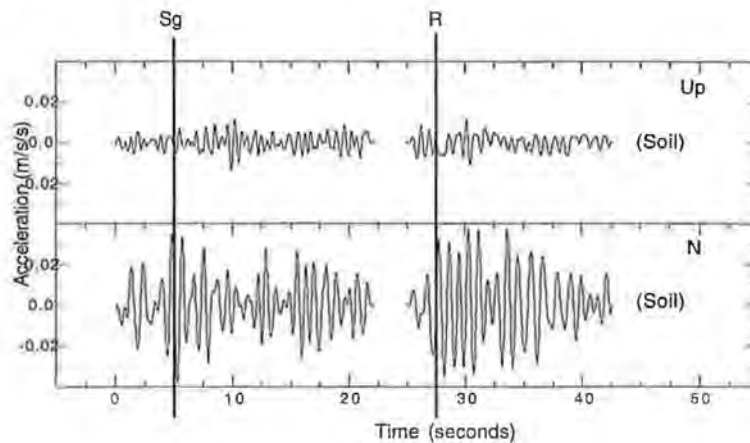

Figure 3. Accelerogram of the 1994 Arthurs Pass earthquake, recorded on deep soft soil in Wainuiomata. The second triggering is at the arrival time of waves travelling at 2.7km/s from the epicentre. R marks the expected arrival time of Rayleigh waves travelling from the epicentre at 2.7km/s, and Sg marks the expected arrival time of the Sg phase.

By itself the record of the Arthurs Pass earthquake merely established that there was resonant motion at the expected time, and this is not entirely surprising as it could merely reflect the dominance of Rayleigh waves at a distance, on rock.
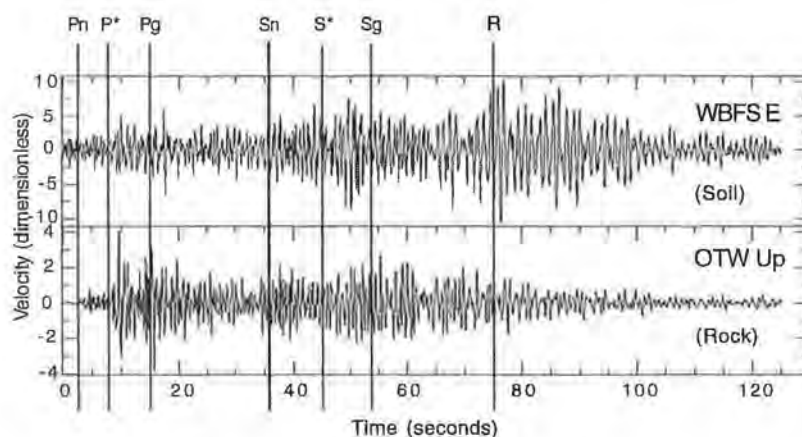

Figure 4. Velocity seismogram of the 1999 Springfield earthquake recorded on deep soft soil at Wainuiomata, and on nearby rock. A strong resonant response is seen for the east component of soil motion at the arrival time of waves travelling at 2.7km/s from the epicentre, but there

is no corresponding increase of rock motion. R marks the expected arrival time of Rayleigh waves travelling from the epicentre at 2.7km/s, and the other vertical lines mark expected arrival times of the refracted crustal phases. OTW senses vertical motion only.

A further recording on the soft soil of the Wainuiomata site and on nearby rock (see figure 4) settles this issue. The 1999 September 14 Springfield earthquake (magnitude 4.5) epicentre was very close to the Arthurs Pass epicentre, and once again resonant motion is seen at the expected arrival time of the Rayeigh waves. However the nearby vertical rock seismogram at station OTW is unremarkable at the Rayleigh arrival time, showing that the Rayleigh wave excites the soil resonance more effectively than do body waves.

6.   IMPLICATIONS

As well as exciting late resonances for distant earthquake sources and prolonging shaking, the same upper-crustal surface waves from closer sources can in principle arrive at the same time as refracted body wave phases, adding to the amplitude of shaking on soft soils for intermediate distances. This effect merits further study.

7.   CONCLUSIONS

This preliminary work suggests that upper-crustal surface waves can propagate in central New Zealand at 2.7km/s for frequencies of around 1Hz, that they are particularly effective at exciting soil resonances, and that their action makes an important contribution to long duration shaking on soft soils.

8.   REFERENCES

Beck, James L. and Hall, John F. (1986) Factors contributing to the catastrophe in Mexico City during the earthquake of September 19, 1985 Geophysical Research Letters,13 (6), p. 593-596.

Begg, J. G., Mildenhall, D. C., Lyon, G. L., Stephenson, W. R., Funnell, R. H., Van Dissen, R. (1993) A paleoenvironmental study of subsurface Quaternary sediments at Wainuiomata, Wellington, New Zealand, and tectonic implications, New Zealand Journal of Geology and Geophysics, 36 (4), p. 461-473.

Chávez-García, F.J., and P.-Y. Bard. (1994) Site effects in Mexico City eight years after the September 1985 Michoacan earthquakes, Int. J. Soil Dynamics and Earthquake Engng, 13, 229-247.

Chavez-Garcia, F.J., Stephenson, W.R. and Rodriguez, M. (1999) Lateral propagation effects observed at Parkway, New Zealand : a case history to compare 1D versus 2D site effects. Bulletin of the Seismological Society of America, 89(3): 718-732

Nakamura, Y. (1989) A method for dynamic characteristics estimation of subsurface using microtremor on the ground surface. QR of RTR 30: 25-33.

Singh, Shri Krishna and Ordaz, Mario (1993) On the origin of long coda observed in the lake-bed strong-motion records of Mexico City, Bulletin of the Seismological Society of America, 83 (4), p. 1298-1306

Stephenson, W.R. (2002) Requirements for verifying wave-wave coupling at Texcoco, Valley of Mexico. Eos, 83(47:supplement): F658.

INFLUENCE OF LAPPED SPLICES ON THE DUCTILITY OF REINFORCED CONCRETE COLUMNS

DR. HELEN GOLDSWORTHY,
SENIOR LECTURER, DEPARTMENT OF CIVIL AND ENVIRONMENTAL ENGINEERING, UNIVERSITY OF MELBOURNE.

AUTHOR:

Dr. Goldsworthy worked as a structural engineer for the firm Skidmore, Owings and Merrill in San Francisco in the early 1980s. On her return to Australia she commenced a Ph.D. under the supervision of Professor L.K.Stevens. In 1987 she was offered a job as a lecturer at the University of Melbourne and has been there ever since.

ABSTRACT:

This paper reports the findings from an experimental program that investigated the influence of lapped splices on the overall displacement capacity of reinforced concrete columns, and compared these with theoretical predictions. The usual Australian practice was followed in the design of the columns in which splices are located immediately above the footing or the floor level. This is only permitted in regions of high seismicity such as New Zealand if the frame is designed using capacity design principles to ensure that the columns are stronger than the beams. Further to this, closely spaced reinforcement must be provided in the lap region. In the design of ordinary moment-resisting frames in Australia, capacity design principles do not have to be adhered to and the spacing of the ties is relatively large.

1 INTRODUCTION

In Australia, reinforced concrete moment resisting frames are a common lateral force-resisting structural system in low to medium rise buildings. Due to the gravity-load dominated nature of these frames and the large spans typically employed for beams, it is likely that, under an extreme earthquake event, plastic hinges will form at the ends of the columns rather than at the ends of the beams at the interior joints, and at the base of the ground floor level columns. In areas of high seismicity with modern design standards such as New Zealand, California and Japan, capacity design principles would typically be used to force the structure to form an energy dissipating mechanism in which the weak links are well defined and the ductility of these links is guaranteed. No such approach is mandatory within the usual practice in Australia.

The experimental and theoretical work presented here investigates whether the critical columns in a case study frame have sufficient ductility to withstand an Australian 500-year return period design-level earthquake. The columns are designed in accordance with AS3600 and contain lapped splices at the base. Previous research focussing on regions of high seismicity has indicated that, in general, lapped splices should not be used in potential plastic hinge locations such as at the base of columns. In those regions, the splices in columns are usually moved up to the middle third of the columns where the moments are low. An exception to this is made if the frame is designed using capacity design principles, [Paulay, 1988], ensuring that the columns are stronger than the beams. In this case, the splices may be located immediately above the floor level, but only if stringent detailing requirements are met. The usual Australian practice is to locate the splices immediately above the floor levels or footings. Since capacity design principles are not generally used, it is likely that plastic hinges will form in some of these locations during an extreme event. The problem is potentially compounded by the lack of strict detailing requirements, especially with regard to the amount and spacing of the transverse reinforcement in these locations.

The aim of this study was to assess the displacement demands likely to be experienced by key column elements in the case study frame if it were subjected to an Australian 500 year return period design level earthquake. Further to this, these were compared with the displacement capacities obtained from the experimental work. Tests were performed on column specimens with and without lapped splices.

2 PREVIOUS STUDIES

In a tension lapped splice, the bond between the concrete and the steel enables the tension force to be transferred through the concrete from one bar to the other. Reversed cyclic loading is much more severe on bond than monotonic loading, especially after yielding of the longitudinal reinforcement has taken place. Bond deterioration can lead to a drop in the stiffness and capacity of the section.

Bond stresses are provided by mechanical interlock of the deformations on the bars and the surrounding concrete. These interlocking forces cause micro-cracks to form in the concrete at the bar deformations, with diagonal compression forces being generated in the concrete between the cracks. Tensile stresses generated by the radial component of

these compressive forces tend to split the concrete along the bar, and must be resisted, in the first instance, by the concrete cover. Yielding of the longitudinal reinforcement causes the micro-cracks to extend and hence lowers the bond resistance. Each yield excursion results in a loss of bond and a further extension of yield penetration into the splice zone. Eventually the tensile stresses in the concrete generated by the radial compressive forces can lead to splitting cracks forming along the bar and spalling of the concrete cover. Spalling of the unconfined cover concrete can also occur when the direction of the frame movement reverses and causes large compressive strains on that side of the column.

When spalling occurs at a splice, the diagonal forces previously applied to the cover concrete are lost. However, it is still possible to develop diagonal compression forces between the spliced bars if sufficient ties are present to provide a clamping force. This truss type mechanism was first proposed in [Paulay, 1982]. [Sivakumar, 1983] concluded that a key aspect in the seismic design of splices is the provision of closely spaced uniformly distributed ties in the splice region.

[Aycardi et al, 1994], and [Lynn et al, 1996] conducted tests on models of reinforced concrete columns with detailing deficiencies reflecting pre-1970s construction in the U.S. The detailing deficiencies included light transverse reinforcement in columns, and lapped splices at the bottom of some of the columns. These column details are not unlike those still used in Australia.

3 ANALYTICAL RESULTS FOR THE CASE STUDY FRAME

The frame chosen was a four-storey ordinary moment-resisting reinforced concrete frame designed and detailed in accordance with AS3600-1988 for a frame in Melbourne on a stiff soil site (S = 1.25). The frame configuration is given in Figure 1 and the reinforcement requirements for the bottom storey columns are given in Table 1.
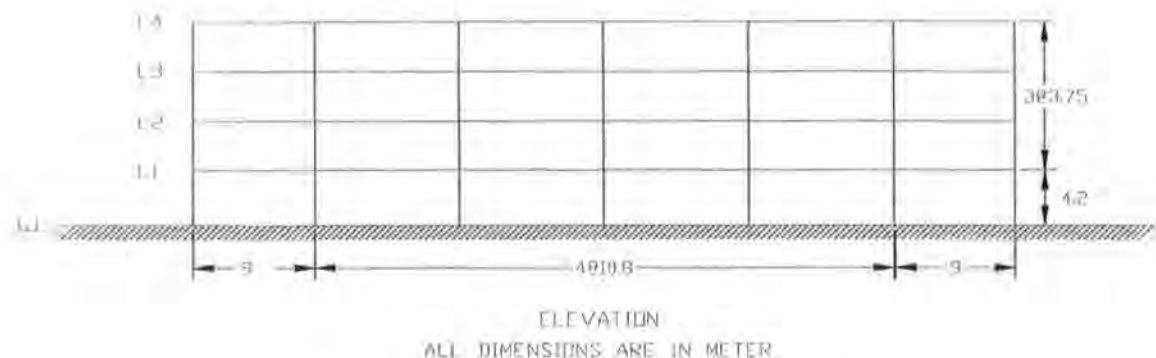

ELEVATION
ALL DIMENSIONS ARE IN METER

Figure 1 - Configuration of the frame

The frame was analysed using the non-linear time-history analysis program Ruaumoko and details of the analysis results are given in [Thiha, 1998]. The accelerograms used as input were 1/3rd El Centro and El Centro. The 1/3rd El Centro input was intended to approximately represent a 500-year return period design-level Australian capital city event, since the response spectra derived from this input gives a good approximation to that in AS1170.4-1993 with an acceleration coefficient of 0.11g. Maximum floor-to-

floor drifts of 16 and 49 mm respectively were found at the ground to 1st floor level. The energy dissipation mechanism was a mixed mode one, leading to significant drifts at all levels. The roof-level displacements were 42 and 89 mm respectively.
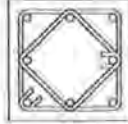
Exterior Columns			Interior Columns		
Level	Size	Steel	Level	Size	Steel
GL to L1	500X500 mm	Main 8 Y28 / Transverse R10 @ 350	GL to L1	500X500 mm	Main 8 Y32 / Transverse R10 @ 350

Table 1 - Details of the column sections

Recent developments in response spectrum modelling [Wilson and Lam, 2003] have led to predictions of the maximum displacement demand for different soil types. For an acceleration coefficient of 0.08g and a 500-year return period, these predictions range from 20 mm (site Class A –hard rock), to 27 mm (site Class B - rock), to 41 mm (site Class C – soft rock or dense soil) and finally to 90 mm (site class E – soft soil). These displacements are the values for a single degree of freedom oscillator. To convert them to roof level displacement, they must be factored by a participation factor. This factor depends on the predominant mode shape and is assumed to be 1.5 for a regular building and 1.0 for a building with a soft storey. The roof-level building displacement of 42 mm obtained above for 1/3rd El Centro is consistent with that at a Class B site (1.5 x 27 = 41 mm). It should be noted, however, that for a 2500-year return period the values for displacements at Class A to Class E sites could increase by a factor of 1.8 [Wilson and Lam, 2003]. For example, at a Class B site with a 2500 year return period, the expected maximum roof displacement would be 41x1.8 = 74 mm.

4 DESIGN OF THE SPECIMENS AND TEST SET-UP

The exterior and interior columns from level GL to L1 were modelled. Initially, four tests were planned, using specimens with splices (S) and without splices (N) to reflect the conditions at the bottom and top of the columns, and with high ($0.35f_c'A_g$, H) or low axial load ($0.15f_c'A_g$, L) to simulate the interior or exterior columns respectively. However, eventually it was decided to use the test results from [Lynn et al., 1996] to represent the no splice-low axial load (Test NL) case. Of necessity, the prototype was scaled down by one third. The same section and reinforcement ratio was used in all of the tests. The prototype and model were assessed to ensure that the level of confining stress provided was very similar for both. Appropriate material properties were used for the concrete and steel in the model, and details can be found in [Thiha, 1998].

The test-rig consisted of a hydraulic actuator suspended vertically from a steel portal frame to apply the axial load to the top of the column specimen. The lateral load was

applied in a quasi-static manner using a jack at a level of 720 mm from the surface of the footing. This level was chosen by assuming that the point of contra-flexure in the column when the frame is subjected to lateral loading would occur at the mid-height of the column. The pattern of lateral loading is given in Figure 2.
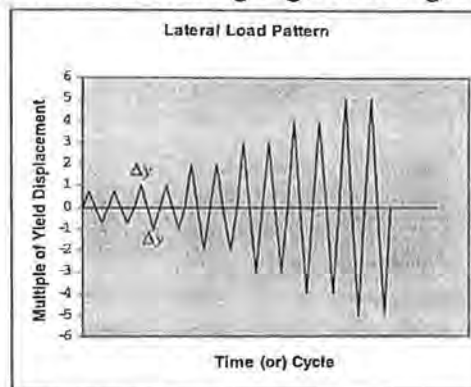

Figure 2 – Lateral Load Pattern

5 TEST RESULTS

The key results that will be reported here are the lateral load vs. horizontal displacement (at the position of lateral load application) envelope curves, the mode of failure and the displacement capacity (at which the lateral load fell to 80% of its maximum value). The envelope curves for all three specimens are given in Figure 3. Flexure rather than shear dominated the behaviour of the columns, and hence all specimens reached their predicted moment capacities. More detailed results including the strains in the transverse and longitudinal reinforcement, the curvature ductility over the plastic hinge length and crack patterns observed throughout the test, can be found in [Thiha,1998].
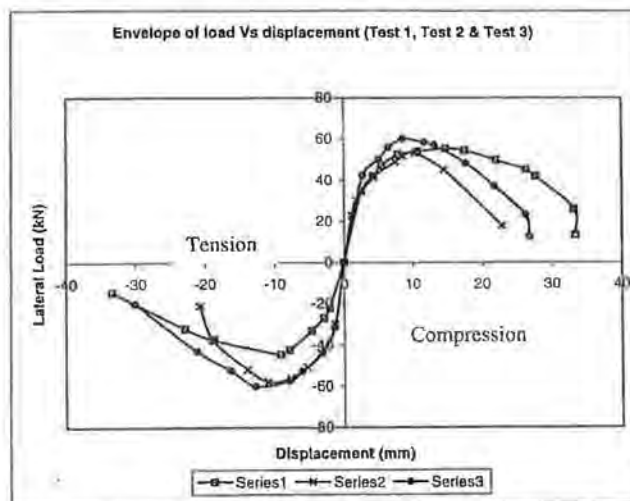

Figure 3 – Load vs. Displacement Envelope Curves

5.1 Test 1 – SL
A maximum load of 54.7 kN was reached. With further cycles of increasing displacement magnitude, the bond between the concrete and the longitudinal steel in the splice region gradually degraded and the peak load dropped. The concrete cover was eventually lost. The lateral load carrying capacity was reduced to almost zero at a

displacement of 33 mm and the test was abandoned. An axial load of 200 kN ($0.15f_c'A_g$) was withstood by the column throughout the test. The displacement of the column at 80% of the maximum load was 27 mm.

5.2 Test 2 – NH

After the maximum load of 54.6 kN was reached, the peak load dropped rapidly with increasing cycles. The concrete cover close to the base of the column spalled early in the test, because of the high level of axial load. During the first cycle towards a displacement of 23 mm, the longitudinal reinforcement suddenly buckled and the axial load carrying capacity was lost. The displacement of the column at 80% of the maximum load was 15.7 mm.

5.3 Test 3 – SH

The behaviour of this specimen was similar to that in Test 1, although there was a steeper drop in the envelope curve after the peak load of 57.6 kN was reached. Despite the high level of axial load, the cover concrete close to the base did not spall off completely until a displacement of approximately 22 mm, compared with a displacement of about 17 mm in Test 2. This is probably due to the sharing of the compression force (due to axial load and bending) between both bars within the splice in Test 3. In Test 3, the axial and lateral load carrying capacities were lost at a displacement of about 26 mm. The displacement of the column at 80% of the maximum load was 17.2 mm.

6 COMPARISON OF ANALYTICAL AND EXPERIMENTAL RESULTS

Since the tests were performed on scaled specimens, the comparison of the results of the analyses on the real frame and the test results are best done using the drift ratio, i.e. the ratio of the relative drift between one level and the next, to the floor-to-floor height. Table 2 compares the test results with the maximum drift ratio obtained in the Ruaumoko analyses.

A worst-case scenario of the ground to first floor becoming a soft storey, and all of the displacement predicted by [Wilson and Lam, 2003] (as discussed in Section 3 of this paper) being concentrated at this level, is also considered for Type C and Type E soil conditions. Both a 500-year and a 2500-year return period are considered, with the latter shown in brackets.

Drift Ratio (%)							
Capacity -Test Results				Demand -Ruaumoko		Demand -Soft Storey	
Test1(SL)	Test2(NH)	Test1(SH)	Lynn*(NL)	$1/3^{rd}$El C	El C	Type C	Type E
3.8	2.2	2.4	2.6	0.4	1.2	1.0(1.8)	2.1 (3.8)

Table 2 – Comparison of drift ratios

7 CONCLUSIONS

The results indicate that the columns, as designed in this case study, should not fail under an Australian 500-year return period design-level earthquake. Even with all of the ground displacement (which corresponds to the maximum displacement of the structure for flexible structures) concentrated in the first floor level, the column behaviour appears to be adequate for a 500-year return period and Type C soil conditions. It is just adequate for Type E soil conditions and a 500-year return period. However, for Type E soil conditions and a 2500 year return period level earthquake, together with the assumption of a soft storey, leading to a drift ratio of 3.8, the frame is likely to suffer total collapse.

The poor behaviour of non-ductile columns in past earthquakes suggests that caution should be exercised in their design. From the experimental results, it is clear that both ends of the columns are at risk, i.e. with the splice or without. In fact, the behaviour of the ends with the splices was marginally better than those without, since buckling was more likely in the case with no splices combined with inadequate transverse reinforcement. Based on previous research, it would clearly be prudent to provide more closely spaced transverse reinforcement. This would serve the purpose of providing extra confinement, reducing the likelihood of buckling and improving the splice behaviour under cyclic loading.

8 ACKNOWLEDGEMENTS

The author is greatly indebted to Swe Thiha, whose Master's thesis forms the basis of the paper. The author has been unable to contact him, but would have liked him to be a joint author.

9 REFERENCES

Aycardi, L.E., Mander, J.B. and Reinhorn, A.M. (1994) Seismic Resistance of Reinforced Concrete Frame Structures Designed only for Gravity Loads; Experimental Performance of Subassemblages, ACI Journal, September-October, pp. 552-563.

Lynn, A.C., Moehle, J.P., Mahin, S.A. and Holmes, W.T. (1996), Seismic Evaluation of Existing Reinforced Concrete Building Columns, Earthquake Spectra, Vol. 12, No. 4, November, pp.715-739.

Paulay, T., (1982), Lapped Splices in Earthquake-Resisting Columns, ACI Journal, November-December, pp. 458-469.

Paulay, T., (1988) Seismic Design in Reinforced Concrete: The State of the Art in New Zealand, Bulletin of the New Zealand National Society for Earthquake Engineering, Vol. 21, No. 3.

Sivakumar, B., Gergely, P., and White, R.N. (1983) Suggestions for the Design of R/C Lapped Splices for Seismic Loading, Concrete International, February, pp. 46-50.

Thiha, Swe, (1998) Influence of Splices on Curvature Ductility within the Column Plastic Hinges, Master's Thesis, Department of Civil and Environmental Engineering, The University of Melbourne.

Wilson, J. and Lam, N. (2003) A Recommended Earthquake Response Spectrum Model for Australia, Australian Journal of Structural Engineering, Vol. 5, No.1.

SHEAR WAVE VELOCITY PROFILING IN MELBOURNE SILURIAN MUDSTONE USING THE SPAC METHOD

JAMES ROBERTS[1] MICHAEL ASTEN[1], HING HO TSANG[2], SRIKANTH VENKATESAN[3], AND NELSON LAM[3]

1. Centre for Environmental and Geotechnical Applications of Surface Waves (CEGAS), School of Geosciences, Monash University, Melbourne, Victoria, Australia.
2. Centre for Earthquake Engineering Research (CEER), Department of Civil Engineering, University of Hong Kong, Pokfulam Road, Hong Kong, SAR, China.
3. Department of Civil & Environmental Engineering, University of Melbourne, Victoria, Australia.

AUTHORS:

James Roberts is a PhD student at Monash University, Melbourne.

Michael Asten is a Professorial Fellow at Monash University part-time and is also a consulting geophysicist and Partner with Flagstaff Geo-Consultants, Melbourne.

Hing Ho Tsang is a PhD student at University of Hong Kong, Hong Kong.

Srikanth Venkatesan is a PhD student at University of Melbourne, Melbourne.

Nelson Lam is a Senior Lecturer at University of Melbourne, Melbourne.

ABSTRACT:

A passive seismic investigation technique known as the spatial auto-correlation (SPAC) method has been used to measure shear wave velocity profiles down to depths of approximately 100m around the Melbourne metropolitan area. A series of surveys have been carried out in different suburbs in Melbourne to develop an average shear wave velocity profile for the bedrock formation. This paper presents details of the surveys including geometries of the geophone arrays, measured auto-correlation spectra, theoretical spectra derived from layered earth models, and the resulting shear wave velocity profiles. These shear wave velocity profiles can be used to assist in modelling the seismic attenuation relationship and radiation damping properties of the bedrock in the area as demonstrated by companion papers presented at this conference.

A passive seismic surveying technique known as the Spatial Auto-Correlation (SPAC) method has been used to measure shear wave velocity (SWV) profiles down to a depth of up to 100m into Silurian mudstone around the Melbourne area. The SPAC technique appears to be well suited to the measurement of SWV profiles in urban areas. Its advantages include its non-invasiveness (no drilling required), speed of data acquisition, low cost and the ability to be able to provide shear wave velocity information over a wide range of depths. In a recent study undertaken jointly by the *Centre for Environmental and Geotechnical Applications of Surface Waves* (CEGAS) at Monash University and the *Earthquake Engineering Research Group* at the University of Melbourne, a series of SPAC surveys were undertaken at five sites around the Melbourne Metropolitan area to develop an average shear wave velocity profile from the surface to an approximate depth of 100-120m.

Major mechanisms amplifying seismic waves as they are transmitted to the ground surface are controlled by the SWV gradient of the earth crust. The effect of this amplification is particularly pronounced on sites covered by soft soil sediments. Consequently, SPAC has been used in previous studies in identifying high hazard sites and modelling the somewhat localised amplification effects of near-surface sediments. The objective of this study, which is distinguished from most of these previous studies (Asten et al, 2003; Asten, 2004), is to model the potential amplification and attenuation properties of seismic waves for the entire region based on measuring and analysing the SWV profiles recorded through thin overburden overlying Silurian mudstone (the basement rock in this region). This new approach of developing regional attenuation relationships is an attractive alternative to conventional modelling methods for regions of low and moderate seismicity where strong motion data is typically lacking.

This paper presents an outline of the basis of the SPAC technique (Section 2); a brief description of the varying geologic conditions within the Melbourne area (Section 3); details of the geophone arrays used (Section 4); measured and theoretical auto-correlation spectra obtained for the Monash University site (Section 5); and a summary of the SWV profiles obtained from each site covered by the study (Section 6). The companion paper (Lam et al, 2004a) presented at this conference, describes the analyses of measured SWV profiles towards the development of the regional attenuation relationship for the Melbourne region. Lam et. al (2004b) [submitted for review to ACMSM conference at Perth, Dec-2004] has presented a methodology to develop seismic attenuation relationships for any region around the globe, based on earth's crustal thickness. The methodology requires information on rock SWV profiles in the top 100m or so. Thus the influence of varied rock SWV profiles at the near surface, on attenuation of seismic waves has now been addressed.

1. BASIS OF THE 'SPAC' METHOD

The SPAC technique measures the propagation of microtremors – very low amplitude ground motions – that occur as the result of both natural (wind, wave action, atmospheric variations) and man-made (road traffic, trains, industrial noise) phenomena. Although the amplitude and frequency content vary with both space and time, microtremors form a background 'field' of (low-amplitude) seismic waves, with most of the energy transported as surface waves. Surface waves are dispersive (i.e. velocity of propagation is dependant upon frequency), with the velocity-frequency relationship being governed (principally) by the shear-wave velocity structure of the earth.

The SPAC technique has as its basis, a mathematical formulation first put forward by Aki (1957) which shows that the azimuthally averaged signal coherency measured using an array of geophones

is related to the velocity-frequency characteristics of the ground beneath the array. By measuring microtremor signal coherency in the field, it is therefore possible to estimate the shear-wave velocity structure in the subsurface over a wide range of depths. Okada (2003) provides a detailed overview of the SPAC technique, while recent studies in Australia (Asten, et al, 2003; Roberts and Asten, 2004) and overseas (Asten, 2004; Apostolidis et al, 2004) have demonstrated the effectiveness of the method in providing shear-wave velocity profiles in a number of different cities.

2. SITE DESCRIPTION

The surveys were carried out at five locations distributed around the Melbourne metropolitan area as shown in Figure 1.
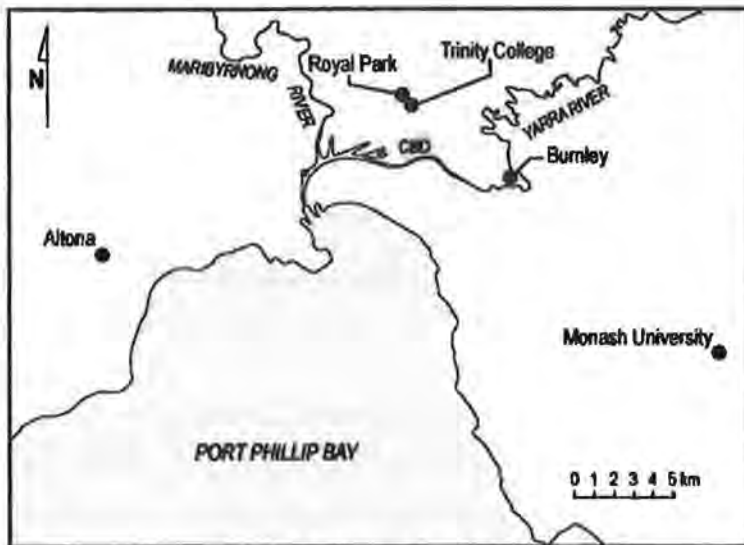

Figure 1: Location of SPAC surveys

The geology of Melbourne and surrounding areas is both complex and variable (Archbold, 1992). Basement rock across Melbourne and surrounding suburbs consists of folded sandstone and siltstone sequences of early to mid-Palaeozoic age (approximately 400 to 450 million years). Although the basement rock is relatively uniform in character, the depth of weathering and extent of jointing is variable (Haustorfer, 1992).

In parts of Melbourne (north, east and northeast of the CBD), this 'basement' rock outcrops at the surface, with no overlying geologic material. This geology is expected at the Royal Park and Trinity College sites indicated in Figure 1. To the north, west and northwest of the CBD, sheets of extrusive basalt rock of variable thickness overly the older basement rocks. The Altona site (Figure 1) is located within this geologic region of Melbourne, while the Burnley survey was undertaken over basalt that constitutes the extreme eastern extent of the basalt. The southeastern suburbs are characterized by significant Tertiary and Quaternary age sediments, consisting of variably consolidated sand, clay and silt which overly the Silurian basement rock. The Monash survey is located in an area that is close to the boundary between these recent sediments and the outcropping basement rock.

3. GEOPHONE CONFIGURATION

SPAC field data consists of time-domain recordings of (vertical, and hence Rayleigh wave) ground motion as measured by an array of geophones. For an array of seven geophones, a hexagonal geometry provides even azimuthal sampling (60 degree spacing) of microtremor energy and is best for situations where microtremor energy is assumed to be propagating evenly from all directions. In situations where a particular direction is likely to account for a greater proportion of the microtremor energy (such as in proximity to a freeway), the array can be placed to 'aim' at the source to better sample the dominant directions of propagation. The 'folded hemisphere' consists of a semi-circular array, consisting of pairs of geophones aligned with an azimuthal spread of 30

degrees. To make this array more compact, one 'half' of the array is offset to lie over the other half in such a way that the most central geophone is common to both halves of the semicircle (as shown in Figure 2).

4. PROCESSING METHODOLOGY

Detailed explanations of the SPAC processing technique are not included in this paper. Readers are directed to references such as Okada (2003) or Asten et al (2004) for general details of the SPAC technique and Asten et al (2003) or Roberts and Asten (2004) for description of the processing and interpretation methodology.

The interpretation of SPAC data consists of fitting the spectra of averaged coherencies measured in the field with the theoretical spectra corresponding to a horizontally layered earth model as governed by equation (1) below.

Routines by Hermann (2001) allow for the dispersion relation, $V(f)$ (Rayleigh wave phase velocity as a function of frequency) to be determined from layered-earth model parameters. Although layer density and compressional (P-wave) velocity contribute to the dispersion relation, shear velocity and layer thickness are the most sensitive model parameters. It can be seen from equation (1) that the resulting (theoretical) coherency spectra should have a form corresponding to a Bessel function, which has the appearance of a decaying sinusoidal waveform.

Figure 2: Geophone array geometries – (a) hexagonal array and (b) "folded hemi" array.

Model parameters (shear velocity and layer thickness) are iteratively varied until the 'best-fit' is achieved between theoretical and measured coherency spectra, as shown in Figure 3 below for data collected on the grounds of Monash University. The solid black line is the field (averaged) coherency curve obtained by processing of the ground motions at each station in the array. The dashed line represents the theoretical coherency curve for the 'best-fit' layered earth model, based upon *fundamental* mode Rayleigh wave motion, which is assumed to be dominant in the frequency range of interest and in the absence of near-sources.
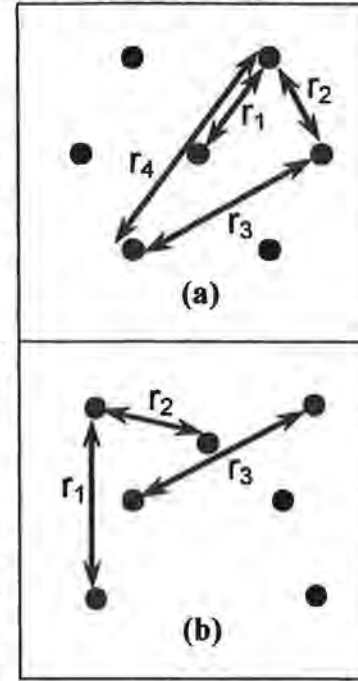
$$\bar{c}(f) = J_0\left(\frac{2\pi f r}{V(f)} \right) = J_0(k.r) \tag{1}$$

where: f is frequency,
$\bar{c}(f)$ is the azimuthally averaged coherency,
J_0 is the zero-order Bessel function,
k is the scalar wavenumber,
$V(f)$ is the velocity dispersion relationship, and
r is the station separation in the circular array.

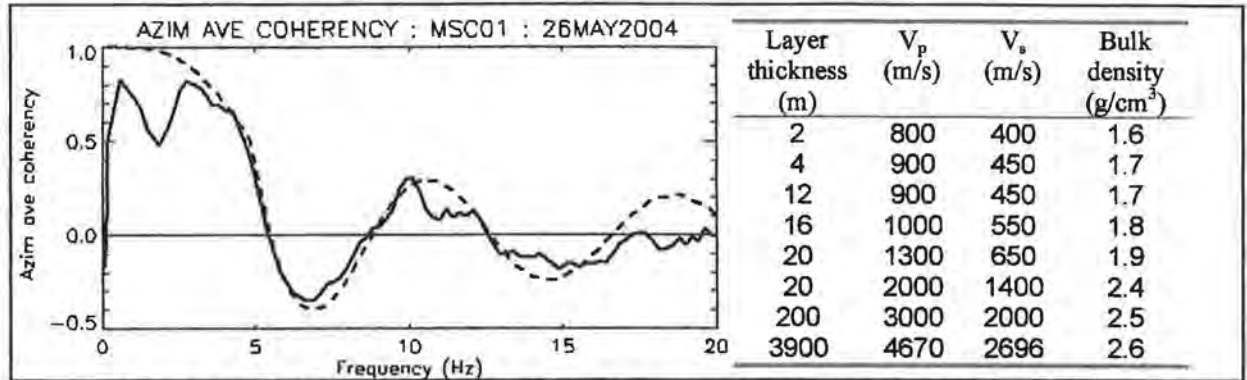| Layer thickness (m)	V_p (m/s)	V_s (m/s)	Bulk density (g/cm³)
2	800	400	1.6
4	900	450	1.7
12	900	450	1.7
16	1000	550	1.8
20	1300	650	1.9
20	2000	1400	2.4
200	3000	2000	2.5
3900	4670	2696	2.6

Figure 3: Sample field (solid line) and theoretical (dashed line) autocorrelation spectra [left]; and corresponding layered earth model parameters for Monash University [right]. Array used was hexagonal (see Figure 2a) with $r_1 = 48$m.

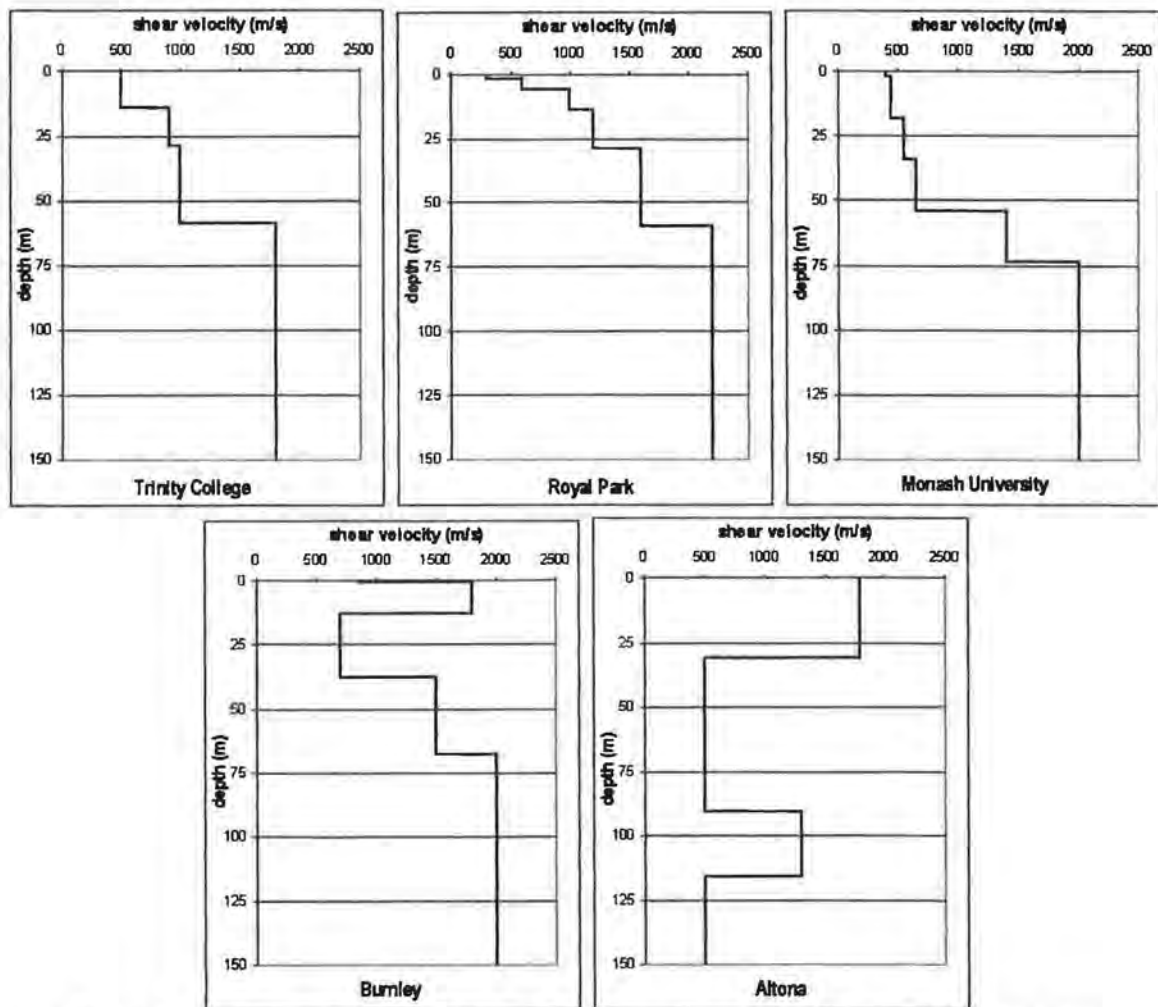## 5. SHEAR WAVE VELOCITY PROFILES FOR CASE STUDY SITES

Figure 4: SWV profiles obtained from SPAC microtremor surveys in the Melbourne area.

Trinity College: Two separate SPAC surveys have been undertaken at this site. An initial survey conducted in September 2003 with hexagonal arrays of 'radius' 17 m and 35 m provided data of insufficient quality to provide definitive results. A more recent survey using the folded hemi array geometry, with a radius of 45 m, provided a significant improvement, allowing the interpretation of the SWV profile, which is indicated for this site in Figure 4. This profile is consistent with the earlier data, but enables determination of the SWV to a depth of approximately 100m. A lack of coherent low frequency microtremor energy and the size of the array limit the reliability of the interpretation below this depth.

Royal Park: Although this site is located less than 1km from the Trinity college site, a significant variation in the interpreted SWV profile can be observed between the two sites. This corresponds with available geological information, which indicates that while Trinity College is located on outcropping Silurian mudstone basement, Royal Park lies in an area where the surface geology is dominated by unconsolidated Tertiary age sandy sediments. A hexagonal array of 48 m radius was adopted for this site to provide the profile in Figure 4.

Monash University: Hexagonal array of 48 m was adopted at this location on a soccer ground. The interpreted SWV profile indicates a significant thickness (<50 m) of relatively soft sediment overlying a higher velocity basement at this site. This result is consistent with geologic maps that indicate that the site lies in an area of poorly consolidated sandy sediments of Tertiary age overlying Melbourne Mudstone.

Altona: At this site, adjacent to Laverton Bowling Club, both a 48 m radius hexagonal array and a coincident 48 m radius folded hemi array were adopted during a SPAC survey undertaken in May 2004. Initial interpretation (under the assumption of fundamental mode Rayleigh wave motion) of this data proved difficult, due to a sharp discontinuity in the coherency curve at a frequency of approximately 4–5 Hz. After more detailed analysis, which identified and addressed the presence of higher mode Rayleigh wave motion, the SWV profile indicated in Figure 4 allowed for a strong agreement between the measured and theoretical coherency curves. This SWV profile is also consistent with geologic cross sections available in this area. This site displays an unusual SWV structure due to a complex geologic structure of alternating layers of (hard) basalt and (soft) sediment.

Burnley: A 48 m radius hexagonal array was adopted for SPAC measurements at this site during October 2003. The resulting SWV profile is quite precisely constrained by relatively high data quality at this site, with velocity and thickness of both the high-velocity layer at the surface and the lower velocity underlying sediments being constrained to within 10-20% of the listed values. More detail on the interpretation of this data can be found in Roberts and Asten (2004). It is observed that the SWV profile (along with that interpreted for the Altona site) shows a high shear velocity layer (basalt) in the upper ten or more meters. In the companion paper however, the basalt layer will be removed in order to provide a general picture of the bedrock structure in Melbourne.

6. CLOSING REMARKS

The usefulness of the SPAC technique in modelling the basement SWV profiles has been demonstrated in this paper based on surveys undertaken on five sites around the Melbourne metropolitan area. The SWV profiles measured from these sites represent considerable variability in the velocity structure of the upper 100 m of the crust around Melbourne. In the companion paper, these SWV profiles are adopted to develop a regional attenuation model for the area. The series of surveys described in this paper represent the first of ongoing attempts to utilize the SPAC technique to measure SWV profiles for use in earthquake hazard studies. Unfortunately, no cone penetrometer results are available for comparison with the SWV profiles obtained using the SPAC technique at the sites in this study. Furthermore, resolution of shear velocities within the basement

rock was limited by thickness of cover and the array size used. With further research and experience in this application of SPAC along with the implementation of larger array sizes, it is expected that more detailed definition of SWV profiles can be developed for the Melbourne area.

7. REFERENCES

Aki, K., (1957) Space and time spectra of stationary stochastic waves, with special reference to microtremors: Bulletin of the Earthquake Research Institute, vol. 35, pp.415-456.

Apostolidis, P., Raptakis, D., Roumelioti, Z., and Pitilakis, K., (2004) Determination of S-wave velocity structure using microtremors and SPAC method applied in Thessaloniki (Greece), Soil dynamics and earthquake engineering. Vol. 24: 49-67.

Archbold, N.W., (1992) Outline of the stratigraphy of the Melbourne area: In: Peck, W.A., Neilson, J.L., Olds, R.J. and Seddon, K.D. (eds), 1992, Engineering Geology of Melbourne: Proceedings of the seminar on engineering geology of Melbourne. Melbourne, Victoria, Australia. Balkema.

Asten, M.W. (2004) Microtremor Array Survey of the Bontany Bay Area, Sydney N.S.W. Report for Geoscience Australia. Monash University.

Asten, M.W., Dhu, T., Jones, A., and Jones, T., (2003) Comparison of shear-velocities measured from microtremor array studies and SCPT data acquired for earthquake site hazard classification in the northern suburbs of Perth W.A. Proceedings of a Conference of the Australian Earthquake Engineering Soc., Melbourne, Paper 12.

Asten, M.W., Dhu, T., and Lam, N. (2004) Optimised array design for microtremor array studies applied to site classification; comparison of results with SCPT logs. Proceedings of the 13th World Conference on Earthquake Engineering, Vancouver.

Asten, M.W., (2004) Method for site hazard zonation, Santa Clara valley: Thickness and shear-velocity mapping of Holocene-Pleistocene sediments by array studies of microtremors. First Annual Northern California Earthquake Hazards Workshop, January 13-14, 2004, USGS, Report, Menlo Park, 2004 (in press).

Haustorfer, I.J., (1992) Engineering properties of Ordovician rocks: In: Peck, W.A., Neilson, J.L., Olds, R.J. and Seddon, K.D. (eds), 1992, Engineering Geology of Melbourne: Proceedings of the seminar on engineering geology of Melbourne. Melbourne, Victoria, Australia. Balkema.

Herrmann, R.B., (2001) Computer programs in seismology - an overview of synthetic seismogram computation Version 3.1: Department of Earth and Planetary Sciences, St Louis University

Lam, N., Asten, M., Chandler, A., Tsang, H., Venkatesan, S. and Wilson, J., (2004a) Seismic Attenuation Modelling for Melbourne based on the SPAC-CAM procedure, Proceedings of a Conference of the Australian Earthquake Engineering Soc., Mount Gambier, [this volume].

Lam, N.T.K., Wilson, J.L., Venkatesan, S., Asten, M., Roberts, J., and Chandler, A.M., (2004b) A generic tool for modelling earthquake hazard, ACMSM 18 conference, Perth, 1-3 Dec 04, [In press].

Okada, H., (2003) The Microseismic Survey Method: Society of Exploration Geophysicists of Japan. Translated by Koya Suto, Geophysical Monograph Series No. 12, Society of Exploration Geophysicists, Tulsa.

Roberts, J. and Asten, M., (2004) Resolving a velocity inversion at the geotechnical scale using the microtremor (passive seismic) survey method. Exploration Geophysics 35 (1), 14-18.

SEISMIC ATTENUATION MODELLING FOR MELBOURNE BASED ON THE SPAC-CAM PROCEDURE

NELSON T.K. LAM[1], MICHAEL W. ASTEN[2], ADRIAN M. CHANDLER[3], HING HO TSANG[3], SRIKANTH VENKATESAN[1] AND JOHN L. WILSON[1]

1. Department of Civil & Environmental Engineering, University of Melbourne, Victoria, Australia.
2. Centre for Environmental and Geotechnical Applications of Surface Waves (CEGAS), School of Geosciences, University of Monash, Melbourne, Victoria, Australia.
3. Centre for Earthquake Engineering Research (CEER), Department of Civil Engineering, University of Hong Kong, Pokfulam Road, Hong Kong SAR, China.

AUTHORS:

Nelson Lam is Senior Lecturer at Department of Civil & Environmental Engineering, University of Melbourne.

Michael Asten is a Principal Research Fellow at Monash University part-time and is also a consulting geophysicist and Partner with Flagstaff Geo-Consultants, Melbourne.

Adrian Chandler is Professor at University of Hong Kong and Director of the Centre for Earthquake Engineering Research in the Department of Civil Engineering.

Hing Ho Tsang is a PhD student at University of Hong Kong, Hong Kong.

Srikanth Venkatesan is a PhD student at University of Melbourne, Melbourne.

John Wilson is Associate Professor at Department of Civil & Environmental Engineering, University of Melbourne.

ABSTRACT:

A pilot study conducted in Melbourne involving shear wave velocity (SWV) profiling in the bedrock formation is used to illustrate a new approach for predicting the potential seismic attenuation characteristics for the region. A complete SWV profile for the entire seismogenic depth of the earth's crust is first developed by combining the SWV profiles measured by the Spatial Auto-Correlation (SPAC) method with regional information provided by a global crustal database. Secondly, the crustal amplification function calculated from the representative SWV profile is combined with predicted attenuation parameter values (*kappa* κ and Q_0) to form a complete filter function representing the potential wave modification characteristics of the earth's crust in the area. Thirdly, a seismic attenuation model is developed by combining this filter function with the source function of the earthquake, using a stochastic procedure and the framework of the Component Attenuation Model (CAM). Lastly, the developed attenuation relationship is compared with seismic Intensity information obtained from three historical earthquakes that affected Melbourne and its surrounding region. The modelling described in this paper only deals with seismic wave modifications within the bedrock formation whilst modifications within the soil sedimentary layers are to be addressed in separate analyses.

1. INTRODUCTION

A passive seismological monitoring technique termed the Spatial Auto-Correlation (SPAC) method has been used to measure shear wave velocity (SWV) profiles down to a depth of some 100 metres into Silurian mudstone around the Melbourne area. Seven surveys were carried out on five sites in different suburbs to develop an average SWV profile for bedrock formations in the area. The companion paper (Roberts *et al.*, 2004) presents details of the surveys including geometries of the geo-phone configurations, measured auto-correlation spectra, theoretical spectra which match with the measured spectra, and the predicted SWV profiles.

In this paper, the typical SWV profiles obtained in the companion paper have been used to develop a seismic attenuation relationship for the city and its suburbs. A complete SWV profile for the entire seismogenic depth of the earth's crust has been developed by combining the representative SWV profile measured by SPAC with regional information provided by the Global Crustal Model: CRUST2.0 (2001). A set of crustal amplification functions so calculated from the representative SWV profile has then been combined with predicted attenuation parameter values (*kappa* κ and Q_0) to form a set of complete filter functions representing the potential wave modification characteristic of the earth's crust in the area. Artificial accelerograms were generated by stochastic simulations based on combining these filter functions with the seismic source function. Velocity response spectra have been computed using the ETAMAC computer program, for a series of magnitude-distance (M-R) combinations, to develop a response spectrum attenuation relationship for the surveyed region. It is noted that the analysis methodology presented herein is based on de-coupling the modification effects of the bedrock from that of the overlying soil sediments. Only mechanisms occurring within the bedrock are addressed in this paper.

The developed attenuation relationship is then presented in terms of the peak ground velocity (PGV) for comparison with values inferred from Modified Mercalli Intensity (MMI) data of three historical earthquakes that affected Melbourne and its surrounding region from long distances, and with magnitudes ranging between 5 and 6.5.

It is noted that the field surveys undertaken so far have been very limited. Thus, the information presented are insufficient to constitute a representative sample for an area. The objective for this paper is to introduce the modelling approach using the pilot study for illustration purposes.

2. CRUSTAL SHEAR WAVE VELOCITY (SWV) PROFILES

Figure 1 summarises all the bedrock SWV profiles obtained in the companion paper (Roberts *et al.*, 2004). A complete representative SWV profile of the earth's crust down to a depth of 8 km has been developed using the procedure described below. Since the effects of the soil sediments are excluded from the modelling and considered in separate analyses, the profiles presented herein are purely within bedrock whilst the upper (soil sedimentary) part of the original profiles have been removed.

On a global scale, the thickness of the upper sedimentary layer can be in the order of tens of metres to a few kilometres. In the region surrounding Melbourne, the thickness of the upper sedimentary layer Z_s has been determined as 500 m using CRUST 2.0(2001), which is also considered as the depth to the surface of the crystalline crustal rock layer Z_c. According to the model SWV profile developed by Chandler $et\ al.$ (2004a), referred herein as the "Chandler's SWV model", the SWV (V_s) variation in the Upper Sedimentary Layer can be expressed in the form shown by equation (1).
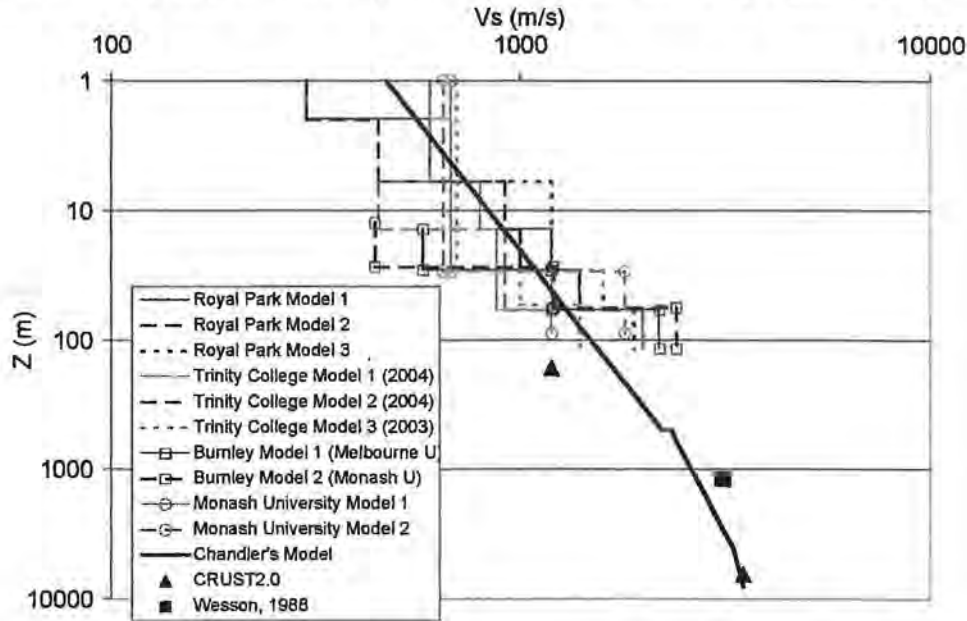

Figure 1   Shear wave velocity (SWV) profiles for the Melbourne area

$$V_{s,C}(Z) = V_{s,30}\left(\frac{Z}{30}\right)^{\frac{1}{4}} \tag{1}$$

In order to obtain the value of $V_{s,30}$, the following formula is proposed

$$\sum \left[\log\left(V_{s,i}(Z_i)\right) - \log\left(V_{s,C}(Z_i)\right)\right] = 0 \tag{2}$$

where $V_{s,i}(Z_i)$ is the SWV at the mid-depth Z_i of each layer from each velocity profile model, whilst subscript "C" denotes Chandler's SWV Model. There are a total of 10 SWV profile models as shown in the above figure with some 46 data points within the upper 100 m. (The depth 100 m is considered to be highly reliable when using the SPAC technique). Using the proposed methodology, $V_{s,30}$ is determined as 1100 m/s.

Together with the regional information obtained from CRUST2.0, $V_{s,8000} = 3500$ m/s, the complete representative bedrock SWV profile can be obtained using the proposed modelling methodology. Hence,

Upper Sedimentary Layer: $V_{s,C}(Z) = 1100\left(\frac{Z}{30}\right)^{\frac{1}{4}}$ $Z < 500m$ \qquad (3a)

Transition Layer: $\qquad V_{s,c}(Z) = 3304 \left(\dfrac{Z}{4000} \right)^{\frac{1}{6}} \qquad 500m < Z < 4000m \quad$ (3b)

Crystalline Crustal Layer: $\quad V_{s,c}(Z) = 3500 \left(\dfrac{Z}{8000} \right)^{\frac{1}{12}} \qquad 4000m < Z \qquad$ (3c)

The proposed SWV model belongs to the same class of model pioneered by Boore & Joyner (1997) which is based on de-coupling amplification effects of the SWV gradient from co-existing attenuation effects arising from energy absorption mechanisms which include wave scattering.

3. DEVELOPMENT OF A REGIONAL SEISMOLOGICAL MODEL

The representative SWV profile modelled in Section 2 has been used to develop a filter function for the earth's crust. This filter function characterising the "path" effects comprises the following four component factors:

(i)   Upper crustal amplification factor $V(f)$
(ii)   Upper crustal attenuation factor $P(f)$
(iii)   All path attenuation factor $Q(f)$
(ii)   Mid crustal amplification factor γ_{mc}

In addition to the enlisted factors, the adopted seismological model has also accounted for factors representing the effects of geometrical attenuation, free-surface amplification, energy partitioning and radiation pattern. Refer Lam et al (2000b) for a review of the seismological model.

The upper crustal amplification factor can be approximated by the "quarter wave-length" rule (Boore and Joyner, 1997) based on the principle of conservation of energy:

$$V = \sqrt{\frac{\rho_A V_A}{\rho_B V_B}} \qquad (4)$$

where ρ_A, ρ_B, V_A and V_B are the densities and SWV respectively, for the media through which shear waves propagate (from medium A to B). A shear wave velocity gradient will result in waves with shorter wave-lengths (ie. higher frequency wave components) being amplified more according to equation 4. The correlation of the amplification factor V with frequency is shown in Figure 2 (refer thin broken line). An increase in the value of V with increasing wave frequency is noted.
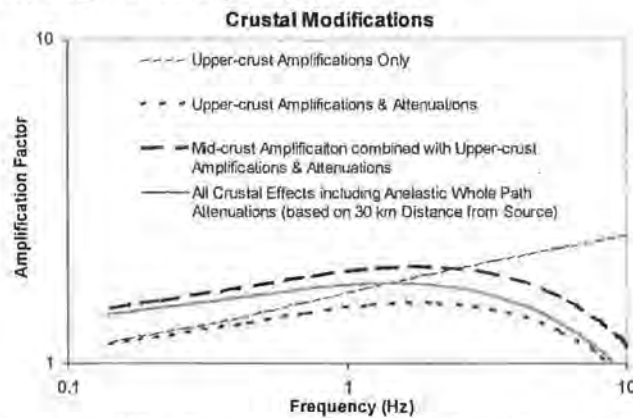

Figure 2   Crustal amplification and attenuation functions for Melbourne area

The upper crustal attenuation factor, which represents the attenuation of waves in the upper 4 km of the earth's crust, is defined by equation (5) (Atkinson and Silva, 1997):

$$P(f) = e^{-\pi f \kappa} \qquad (5)$$

where the parameter κ (*kappa*) can be measured from analysis of the Fourier transform of seismic waves recorded from the very near-field (Anderson and Hough, 1984). Recommendations for the value of κ have been made for California, British Columbia and various regions in Europe (as summarized in Chandler *et al.* 2004b), but information available in regions of low and moderate seismicity around the world remains very restricted. In view of this and difficulties in capturing near-field data, a model which relates the κ parameter and the SWV of the earth's crust has been developed by Chandler *et al.* (2004b), and is referred herein as the Chandler's Kappa Model. This model was developed from empirical curve-fitting in conjunction with analytical modelling and is based on the premise that the lower the SWV of the earth's crust, the higher the level of energy absorption. Factors affecting the value of κ other than SWV are manifested by scatter in the correlation (refer Figure 3). According to Chandler's Kappa Model, a κ value of 0.033 is inferred by a SWV of $V_{s,30} = 1.1$ km/sec. Substituting $\kappa = 0.033$ into equation (5) gives the frequency-dependent crustal attenuation function, which is combined with the amplification function obtained above.
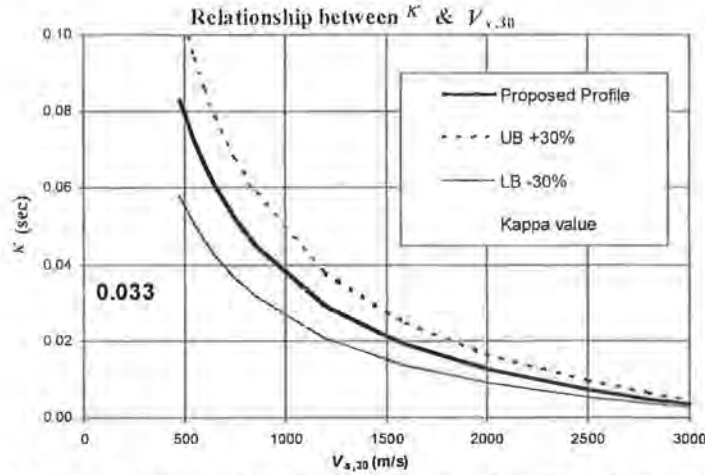

Figure 3   Determination of the κ parameter (after Chandler *et al.* 2004b)

Next, the whole path attenuation factor $An(f)$ which is defined by equation (6) is considered.

$$An(f) = e^{\frac{\pi f R}{Q \beta}} \qquad (6)$$

In the study by Chandler *et al* (2004b), Q_o (Q at 1 Hz) is estimated at 278 based on the measured SWV. This estimated value for Q_o is interestingly comparable to the value of 204 estimated for California (Atkinson and Silva, 1997). The $Q(f)$ function for Melbourne is then defined by equation (7) with the exponent value of "0.6" estimated in accordance with the recommendations by Mak *et al* (2004) :

$$Q(f) = 278(f)^{0.6} \qquad (7)$$

Substitution of equation (7) into equation (6) gives the estimated whole path attenuation factor for the Melbourne region (refer Figure 2). Finally, the mid-crustal amplification factor for SWV of 3.5 km/sec at the source of the earthquake (taken at 5 - 8 km depth) is estimated at 1.3 (Lam et al. 2000a). Each of the filter functions representing various crustal modification effects are shown in Figure 2, along with the combined filter function which accounts for all crustal effects (but not including geometrical attenuation).

4. STOCHASTIC GROUND MOTION SIMULATIONS

The crustal filter function developed in Section 3 has been combined with the generic intraplate source model of Atkinson (1993) to define the frequency contents of future earthquakes affecting the Melbourne area. Artificial accelerograms were simulated stochastically using the computer program GENQKE (Lam et al. 2000b). The response spectra calculated from some 18 accelerograms with random phase angles were averaged for a series of magnitude-distance (M-R) combinations, as shown in Figure 4.

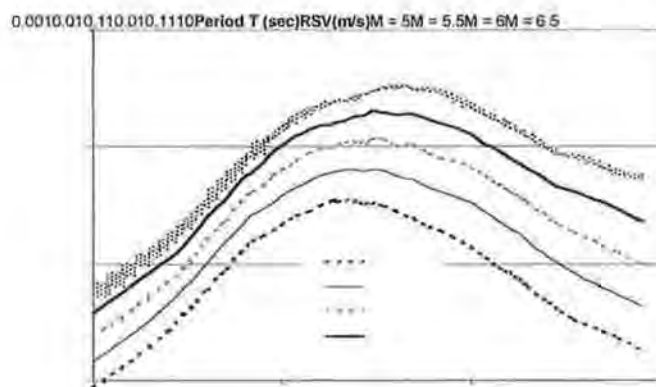0.0010.010.110.010.1110Period T (sec)RSV(m/s)M = 5M = 5.5M = 6M = 6.5

Figure 4 Response spectra for a series of M-R combinations (R=30km)

Finally, the attenuation relationship developed for Melbourne using the SPAC-CAM methodology presented in this paper is shown in terms of the peak ground velocity (PGV) in Figure 5. The PGV was taken as the highest response spectral velocity divided by 1.8 according to Wilson and Lam (2003) citing the work of Somerville et al (1998). Superimposed onto Figure 5 are PGV's inferred from MMI data of three historical earthquakes which affected Melbourne (McCue, 1995). Refer legend in Figure 5 for details. The transformation from MMI to PGV (mm/sec), was based on recommendations by Newmark and Rosenblueth (1972) as defined by equation (8).

$$2^{MMI} = \frac{7}{5}PGV \quad (PGV \ in \ mm)$$ (8)

It is shown in Figure 5 that the recorded (and inferred) PGV's and the modelled PGV's have discrepancies by a factor of 1.2-1.7 at 100km distance (which is equivalent to approximately half an MMI unit). Such discrepancies can be explained by the fact that the modelled PGV's are based on rock conditions whereas the PGV's inferred from MMI data refer to average site conditions. The objective of comparing the two sets of data is simply to show that they do not contradict in terms of order of magnitude.
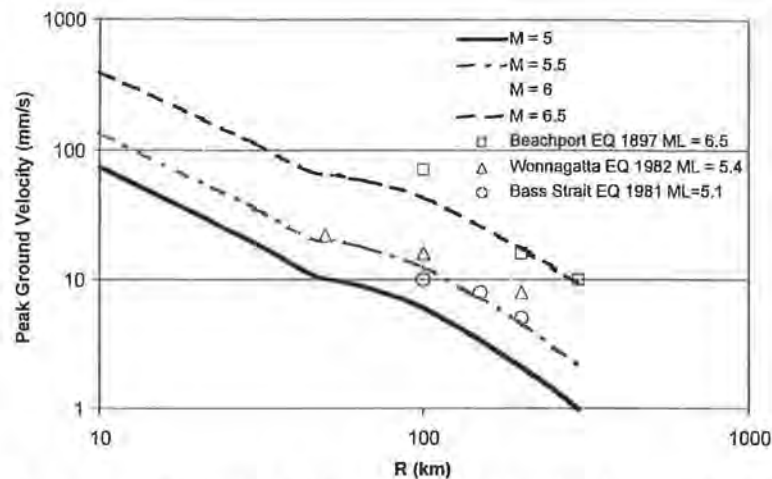
Figure 5 Peak Ground Velocity (PGV) attenuation relationship developed for Melbourne

5.   CONCLUSIONS

- A pilot study is described in this paper to illustrate a new approach for determining the SWV profile for the bedrock formation in an area. Field measurements using SPAC technique were used in conjunction with seismic refraction data reported for the Melbourne area and subsequently incorporated into the Global Crustal Model.
- Crustal amplification factors were calculated from the modelled representative SWV profile using the quarter-wavelength rule and attenuation functions calculated in accordance with correlations developed for the κ and Q_0 parameters.
- Filter functions characterising the crustal amplification and attenuation effects in the bedrock formation were obtained.
- Artificial accelerograms (hence response spectra) were then generated by stochastic simulations based on the calculated filter functions to develop a PGV attenuation relationship for average rock sites in Melbourne. The developed relationship does not contradict with inferences from historical MMI data.

6.   REFERENCES

Anderson, J.G. and Hough, S.E. (1984) A model for the shape of the fourier amplitude spectrum of acceleration at high frequencies, Bulletin of the Seismological Society of America, Vol 74, No 5, pp 1969-1993.

Atkinson, G.M. (1993) Earthquake source spectra in Eastern North America, Bulletin of the Seismological Society of America, Vol 83, pp 1778-1798.

Atkinson, G.M. and Silva, W. (1997) An empirical study of earthquake source spectra for Californian earthquakes, Bulletin of the Seismological Society of America, Vol 87 pp 97-113.

Boore, D.M. and Joyner, W.B. (1997) Site amplifications for generic rock sites, Bulletin of the Seismological Society of America, Vol 87, No 2, pp 327-341.

Chandler, A.M., Lam, N.T.K. and Tsang, H.H. (2004a) Shear wave velocity modelling in bedrock for analysis of intraplate seismic hazard, Soil Dynamics and Earthquake Engineering, accepted for publication and in-press.

Chandler, A.M., Lam, N.T.K., Tsang, H.H. and Sheikh, M.N. (2004b) Estimation of near-surface attenuation in bedrock for analysis of intraplate seismic hazard, International Journal of Seismology and Earthquake Engineering, Submitted February 2004.

Global Crustal Model CRUST2.0. (2001) Institute of Geophysics and Planetary Physics, Univ. of California, San Diego. http://mahi.ucsd.edu/Gabi/rem.dir/crust/crust2.html

Lam, N.T.K., Wilson, J.L., Chandler, A.M. and Hutchinson, G.L. (2000a) Response spectral relationships for rock sites derived from the component attenuation model, Journal of Earthquake Engineering & Structural Dynamics, Vol 29, pp. 1457-1489.

Lam, N.T.K., Wilson, J.L. and Hutchinson, G.L. (2000b) Generation of synthetic earthquake accelerograms using seismological modeling: a review, Journal of Earthquake Engineering, Vol 4, No 3, pp. 321-354.

Mak S., Chan L.S., Chandler A.M. and Koo R.C.H. (2004) Coda Q Estimates in the Hong Kong Region, *Journal of Asian Earth Sciences*. Accepted and In press.

McCue, K. (1995). *Atlas of Iso-seismal Maps of Australian Earthquakes : Part 3.* Geoscience Australia publication record Vol.55(44); original source of information from Australia Geological Survey Organisation.

Newmark, N.M. and Rosenblueth, E. (1971) Fundamentals of earthquake engineering. Prentice-Hall, New Jersey.

Roberts, J., Asten, M.W., Tsang, H.H., Venkatesan, S. and Lam, N.T.K. (2004) Shear Wave Velocity Profiling in Melbourne Silurian Mudstone Using the SPAC Method, Proceedings of a Conference of the Australian Earthquake Engineering Society (AEES), Mount Gambier, South Australia. Submitted.

Somerville, M., McCue, K. and Sinadinovski, C.. (1998). Response Spectra Recommended for Australia, *Procs. Australian Structural Engineering Conference,* Auckland: pp.439-444.

Wesson, V. (1988) Seismic modelling of the Victorian lithosphere, MAppSc Thesis, Phillip Institute of Technology, Victoria, Australia.

Wilson, J.L. and Lam N. (2003) A Recommended Earthquake Response Spectrum Model for Australia, *Australian Journal of Structural Engineering,* Vol.5 (1), pp. 17-28.